UPPSALA
UNIVERSITET

Digital Comprehensive Summaries of Uppsala Dissertations from the Faculty of Science and Technology 232

Wave Energy Conversion

Linear Synchronous Permanent Magnet Generator

OSKAR DANIELSSON

ACTA
UNIVERSITATIS
UPSALIENSIS
UPPSALA
2006

ISSN 1651-6214
ISBN 91-554-6683-4
urn:nbn:se:uu:diva-7194

Dissertation presented at Uppsala University to be publicly examined in Siegbahnsalen, Ångströmlaboratoriet, Box 534, Uppsala, Friday, November 10, 2006 at 13:15 for the degree of Doctor of Philosophy. The examination will be conducted in English.

Abstract
Danielsson, O. 2006. Wave Energy Conversion. Linear Synchronous Permanent Magnet Generator. Acta Universitatis Upsaliensis. *Digital Comprehensive Summaries of Uppsala Dissertations from the Faculty of Science and Technology* 232. 102 pp. Uppsala.
ISBN 91-554-6683-4.

This thesis studies the electric aspects of a linear synchronous permanent magnet generator. The generator is designed for use in a wave energy converter, which determines the fundamental requirements of the generator. The electromagnetic properties of the generator are investigated with a finite element based simulation tool. These simulations formed the base of the design and construction of a laboratory prototype. Several experiments where conducted on the prototype generator. The results verify at large the simulation tool. However, a difference between the measured and simulated air gap flux was discovered. This was attributed to the longitudinal ends of the generator, which are ignored in the simulation tool. Experiences from the construction, and further finite element studies, led to a significant change in the support structure of the first offshore prototype generator. A complete wave energy converter was constructed and launched, the 13th of March, on the west coast of Sweden. A study of the load resistance impact on the power absorption has been carried out. An optimal load interval, with regard to power absorption, has been identified. Furthermore, the generator has proofed to withstand short term overload several times larger than the nominal load. Finally, the longitudinal ends' influence on the flux distribution was investigated with an analytical model, as well as finite element simulations. A possible problem with large induction of eddy currents in the actuator back steel was identified.

This work is a part of a larger project, which aims do develop a viable wave energy conversion system.

Keywords: Finite element method, linear synchronous generator, longitudinal end effect, permanent magnet, point absorber, offshore testing, wave power

Oskar Danielsson, Department of Engineering Sciences, Division for Electricity and Lightning Research, Box 534, Uppsala University, SE-75121 Uppsala, Sweden

ISSN 1651-6214
ISBN 91-554-6683-4
urn:nbn:se:uu:diva-7194 (http://urn.kb.se/resolve?urn=urn:nbn:se:uu:diva-7194)

To Karin

List of Papers

This thesis is based on the following papers, which are referred to in the text by their Roman numerals.

I **Danielsson, O.**, Leijon, M., and Sjöstedt, E. "Detailed Study of the Magnetic Circuit in a Longitudinal Flux Permanent-Magnet Synchronous Linear Generator" (2006) *IEEE Transactions on Magnetics*, volume (41), No (9), pp.2490–2495

II **Danielsson, O.**, Eriksson, M., and Leijon, M. "Study of a longitudinal flux permanent magnet linear generator for wave energy converters" (2006) *International Journal of Energy Research*, in press, available online, Wiley InterScience

III **Danielsson, O.**, Stålberg, M., and Leijon, M. "Verification of Cyclic Boundary Condition and 2D Field Model for Synchronous PM Linear Generator " *Submitted to IEEE Transaction on Magnetics*, September (2006)

IV Waters, R., Stålberg, M., **Danielsson, O.**, Svensson, O., Gustafsson, S., Strömstedt, E., Eriksson, M., Sundberg, J., and Leijon, M. (2006) "First experimental results from sea trials of a novel wave energy system" *Submitted to Applied Physics Letter*, September (2006)

V **Danielsson, O.** and Leijon, M. "Analytic model of flux distribution in linear PM synchronous machines including longitudinal end effects" *Accepted, IEEE Transaction on Magnetics*, July (2006)

VI Nilsson, K., **Danielsson, O.**, and Leijon, M."Electromagnetic forces in the air gap of a permanent magnet linear generator at no load" (2006) *Journal of Applied Physics*, volume (99), No (3), pp.1–5

VII Waters, R., **Danielsson, O**., and Leijon, M."Measuring air gap width of permanent magnet linear generators using search coil sensor" (2006) *Accepted, Journal of Applied Physics*

VIII Leijon, M., **Danielsson, O.**, Eriksson, M., Thorburn, K., Bernhoff, H., Isberg, J., Sundberg, J., Ivanova, I., Ågren, O., Karlsson, K.E., and Wolfbrandt, A. (2006) "An electrical approach to wave energy conversion" *Renewable Energy*, volume (31), issue (9), pp. 1309-1319

IX **Danielsson, O.**, Sjöstedt, E., Thorburn, K., Leijon M.,"Simulated Response of a Linear Generator Wave Energy Converter" *Proceedings of ISOPE 2004*, Toulon, France

X **Danielsson, O.**, Leijon M., Thorburn, K., Eriksson, M., Bernhoff, H. "A direct drive wave energy converter - Simulations and experiments" *Proceedings of OMAE 2005*, Halkidiki, Greece

Reprints were made with permission from the publishers.

Contents

1 Introduction 13
1.1 Wave energy 14
1.1.1 The resource 14
1.1.2 Wave energy engineering 16
1.1.3 Direct drive vs conventional generators 17
1.2 The wave energy converter concept 18
1.3 Aim of thesis 19
2 Theory 21
2.1 Electromechanical energy conversion 21
2.2 Linear permanent magnet synchronous generator 22
2.2.1 Lumped circuit of synchronous generator 23
2.2.2 Induced emf 25
2.2.3 Synchronous inductance 26
2.2.4 Armature flux 27
2.3 Maxwell's equations 30
2.4 Magnetic materials 30
2.4.1 Soft ferromagnetic materials 33
2.4.2 Permanent magnet material 34
2.5 Losses 34
2.5.1 Copper losses 34
2.5.2 Eddy currents 35
2.5.3 Hysteresis losses 37
2.5.4 Excess losses 37
2.6 Influence of non-linearities in electric machines 37
2.7 Finite element modeling 38
2.7.1 Field formulation 38
2.7.2 Cyclic boundary condition and internal moving boundary 39
2.7.3 Magnetic material modeling 40
2.8 Longitudinal end effect model 41
3 Linear generators 47
3.1 Differences between linear and rotating generators 47
3.2 Basic conditions 48
3.3 Linear generators for wave energy conversion 50
3.4 Longitudinal Flux PM Generator 50
3.4.1 Cable winding 51
3.4.2 Permanent magnets 52

3.4.3 Stator steel 52
4 Design 55
4.1 Finite element based design 55
4.2 General design considerations 56
4.3 Load current 57
4.4 Magnetic circuit 57
4.4.1 Numbers of cables per slot 58
4.4.2 Pole width 59
4.4.3 Permanent magnet design 59
4.4.4 Stator steel geometry 60
4.5 Design of test generator 60
5 Experimental generator 63
5.1 Construction 63
5.1.1 Stator cable winding 64
5.1.2 Normal air gap forces 65
5.2 Experiments 66
5.2.1 Magnetic field distribution 66
5.2.2 Slow speed 66
5.2.3 Nominal speed 67
5.3 Air gap width measurement sensor 67
6 Full scale offshore experiments 69
6.1 The wave power plant 69
6.1.1 Generator 70
6.1.2 Electric system 71
6.2 Measurements 72
6.3 Power absorption for different damping factors 74
7 Longitudinal ends 75
7.1 Static longitudinal end effect 75
7.2 Analytic reluctance model 77
7.3 Finite element simulations 78
7.4 Consequences 78
8 Discussion 81
8.1 Design 81
8.2 Experiments 82
8.3 Offshore experiments 84
8.4 Longitudinal end effect 85
9 Conclusion 87
10 Summary of papers 89
11 Svensk sammanfattning 93
12 Acknowledgment 95
Bibliography 97

Nomenclature and abbreviations

$\mathbf{A}$	Tm	Magnetic vector potential
$\mathbf{B}$	T	Magnetic field
$\mathbf{D}$	C/m^2	Displacement field
$\mathbf{E}$	V/m	Electric field
$\mathbf{H}$	A/m	Magnetic field
$\mathbf{J}_f$	A/m^2	Free current density
$\mathbf{J}_m$	A/m^2	Magnetization current density
$\mathbf{K}_s$	A/m	Surface current dens.
$\mathbf{M}$	A/m	Magnetization field
A_{air}	m^2	Air gap area
A_c	m^2	Conductor area
A_z	Tm	z-component of magnetic vector potential
B	T	Magnetic induction
B_a	T	Magnetic induction of armature flux wave
B_{ph}	T	Magnetic induction of phase flux wave
B_r	T	Remanent magnetic induction
B_s	T	Saturation magnetic induction
C_c	F	Sea-cable capacitance
d_{steel}	m	Thickness of steel
d_{coat}	m	Thickness of insulation
E	V	Electromotive force
F	N	Force
F_g	N	Air gap force
H_c	A/m	Coercive field strength
H_{ic}	A/m	Intrinsic coercive field strength
h_{mag}	m	Magnet height
H_s	m	Significant wave height
I	A	Current
I_{enc}	A	Enclosed current
I_{ph}	A	Phase current
I_{pm}	A	PM-current, current sheet approach

J	A/m^2	Current density
J_{pm}	A/m^2	PM-current density, current sheet approach
J_s	A/m^2	Source current density
k_e	$Js^{1/2}/(m^3T^{3/2})$	Excess loss material constant
k_{damp}	Ns/m	Damping factor
k_h	$J/(m^3T^2)$	Hysteresis loss material constant
k_s	–	Stacking factor
L	H	Inductance
L_c	H	Sea cable inductance
l_c	m	Cable length
L_l	H	Leakage inductance
L_m	H	Main inductance
L_s	H	Synchronous inductance
l_{stack}	m	Stack length
M	A/m	Magnetization
mmf_{pm}	A-turns	Permanent magnet magnetomotive force
M_r	A/m	Remanent magnetization field
$\hat{\mathbf{n}}$	–	Normal unit vector
N_{pole}	–	Number of poles
N_{turns}	–	Number of coil-turns per poles
P	W	Power
p_{eddy}	W/m^3	Eddy current loss density
p_{excess}	W/m^3	Excess loss density
$p_{hysteres}$	W/m^3	Hysteresis loss density
P_{ohm}	W	Ohmic losses
p_{ohm}	W/m^3	Ohmic losses density
R_c	Ω	Sea cable resistance
R_g	Ω	Stator winding resistance
R_l	Ω	Load resistance
q	–	Slot/pole & phase
t	s	Time
T_p	s	Peak period
U_{even}	J	Magnetic energy, even number of magnets
U_{mag}	J	Magnetic energy
u_{mag}	J/m^3	Magnetic energy density
U_{odd}	J	Magnetic energy, odd number of magnets
v	m/s	Speed
w_{air}	m	Air gap width
w_{coil}	m	Coil width

w_{mag}	m	Magnet width
w_{pole}	m	Pole width
w_{tooth}	m	Tooth width
w_{tip}	m	Tooth tip width
w_{waist}	m	Slot waist width
$W_{electric}$	J	Electric energy
W_{field}	J	Field energy
W_{loss}	J	Loss energy
$W_{mechanic}$	J	Mechanic energy
x'	m	Actuator position
x_i	–	Free parameter, reluctance model
X_s	Ω	Synchronous reactance
V	V	Voltage
V_l	V	Load voltage
χ_m	–	Magnetic susceptibility
δ	°	Load angle
δ_s	m	Skin depth
Φ	Wb-turns	Flux linkage
ϕ	Wb	Flux
ϕ_{pm}	Wb	Permanent magnet induced flux
μ_0	Vs/Am	Permeability of vacuum
μ_r	–	Relative permeability
μ_{rec}	–	Recoil permeability.
σ	A/Vm	Conductivity
ω	rad/s	Angular frequency
$\Re$	1/H	Reluctance
$\Re_{i1}$	1/H	Reluctance, reluctance model
$\Re_{i2}$	1/H	Reluctance, reluctance model
σ_f	C/m^3	Free charge density

AC	Alternating Current
DC	Direct Current
emf	Electromotive force
FE	Finite Element
LNG	Liquid Natural Gas
Nd–Fe–B	Neodymium–Iron–Boron
PM	Permanent Magnet
r.m.s.	Root mean square
TFPM	Transversal Flux Permanent Magnet
VRPM	Variable Reluctance Permanent Magnet

1. Introduction

The concern for the world's future good is intimately linked with our civilization's need for energy. Energy is by far the largest merchandise in the world and an enormous amount of energy is extracted, distributed, converted, and consumed in our global society daily. Meanwhile scientists all over the world is debating whether the oil production has reached its peak [1, 2, 3] and if the humanity's carbon dioxide emissions are affecting the climate of the Earth [4, 5], the global energy demand is continuously increasing. The fact that 83% of the energy production is based on fossil fuel [6], worries some people more than others. Most of us agree, however, that sometimes in the future the world will need to switch into a sustainable energy system. The question is when? When do we need to take on the enormous challenge, and when will it be too late at some point? The risks we are facing as we bide our time are not only environmental but to a great extent economical and political. A global energy shortage will have devastating consequences on the stability and economy of the world.

Energy shortage is forcing several countries to redirect their energy system and we have today a unique situation where we can influence the direction of the future energy systems. Chile is a good example [7]. Chile's energy consumption is steadily increasing and the country has for several years been dependent on gas supplies from Argentina. When Argentina in 2004 began shutting down the gas supplies to Chile, mainly because of shortage of gas in the domestic market, Chile was faced with an energy crisis. Chile is now in progress to find new sources of energy to match the increasing consumption and they will most probably go for the *liquefied natural gas* (LNG) alternative. Billions of dollars will be invested in infrastructure and Chile will have their future energy system locked in an LNG dependence for several decades. Unfortunately, Chile is not the only country interested in LNG [8] and there are signs indicating that LNG production already today has problems with rising costs and opposition from public opinion. Chile will not only contribute to the carbon dioxide emission of the world, but risk facing another energy crisis as LNG gets scarce and prices goes up. There are however alternatives. Chile has a coast 4000 km long facing the Pacific Ocean. The annual amount of energy that is carried by ocean waves and hits the coast is more than 20 times greater than the total energy consumption of Chile. Imagining a little part of that energy being harvested, in combination with the large amount of domestic hydropower production, they could build an energy system with a

large content of renewable energy sources. Their dependence on fossil fuel import would decrease drastically.

Chile has an exceptionally energetic wave climate, but a more moderate wave climate such as the Baltic Sea [9] [10] could provide a considerable amount of energy to the surrounding countries.

One part of the challenge is the engineering. Before we can capture any of the vast amount of wave energy in the oceans we need to find engineering solutions that in an economic and safe way converts the energy of the waves into useful energy for the society. Before any society will choose this alternative way for their future energy system, the viability of the technology must be proved.

1.1 Wave energy

The first real attempts to construct wave energy converters were made in the 1970s, when the oil crisis caused a sudden interest in finding complementary sources of energy. The scientists where virtually starting from scratch, and it took years to build a knowledge base and to gain experiences [11, 12]. But trouble have followed. Machines made to absorb the power of the waves tend to break. And when you build a machine that can withstands the forces, it tends to be way to costly. Many doubted that it would ever be possible to extract the wave energy in an economic way and, as oil prices sank, the funding for way energy research was discontinued.

In the end of the 1990s the interest was reborn and several government funded R&D schemes were initiated with the United Kingdom in the lead. Today it seems like we are approaching a breakthrough. Several research projects have reached the full scale testing stage [13] and the first commercial projects have been scheduled [14].

However, a lot of questions remain, and wave energy technology is far from reaching a consensus on the most appropriate way to harvest the energy of the oceans. The quest to conquer the forces of the ocean waves has just begun!

1.1.1 The resource

It is the natural source that sets the fundamental prerequisites for renewable energy conversion. Compared with other renewable energy sources wave energy has several interesting properties, such as high power density, high availability, and a large resource. There are also complicating factors such as a large variation in power, harsh environment, and difficult access.

Wave power is a converted and concentrated form of solar power. Wind energy is a product of temperature gradients caused by the sun acting over a large area over a long period time. In turn, waves are a product of long-term influence of wind energy upon the surface of large bodies of water. The power

Figure 1.1: Average annual power density of ocean waves [kW/m]

density in ocean waves are often an order higher than wind and orders higher than solar power. The average annual power densities of ocean waves of the world are illustrated in Fig. 1.1. The power density is given in *kilo watt per meter*, which is the energy transport per time over a line perpendicular to the direction of the waves. The highest powers are found on the west coasts of the continents facing the large oceans in the 40 – 60 latitude range. The total wave energy resource of the oceans of the world is, in a conservative study, estimated to 2 TW [15].

The availability of an energy source is an important economic factor since the incomes for an electricity producing plant are governed by the *average energy production*, whereas the investments costs to a great extent are determined by the maximum power, *i.e.* the *rated power*, of the plant. This is expressed by the *utility factor*, which is the quotient between the rated power and the average energy production [16]. Ideally an energy plant is producing at rated power all the time, but for renewable energy sources the availability is limited by the natural fluctuation of the source. Wave energy has, however, one of the largest utility factors of the renewable energy sources. This is due to the storage and transport capacity of ocean waves — even when the wind ceases the waves continue to roll and storm waves can be transported several thousands of kilometers, hitting the coast days after the storm is over.

Another encouraging factor is the that the energy extraction can be carried out with low negative interaction with the surroundings. According to the Electric Power Research Institute, wave power is one of the most environmentally benign ways to generate electricity [17]. Furthermore, offshore wave energy plants have a relatively low profile, and have low visual impact from the shore. Visual disturbance and public acceptance are not negligible factors, which have hindered the development of many energy projects, such as nuclear, coal, and wind generation.

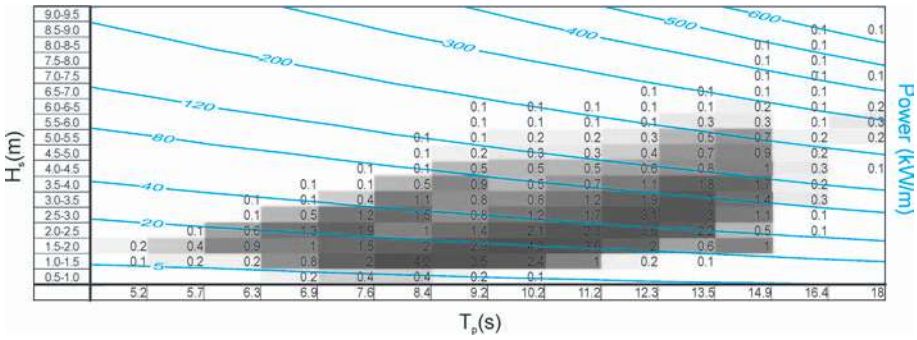

Figure 1.2: Scatter diagram from the Atlantic Ocean outside of Portugal, the occurrence of every wave condition is given in percentage of the year

There is obviously a number of attractive characteristics to the wave energy source but there are also some obstacles. One big challenge is how to handle the large variation in power. Figure 1.2 shows a *scatter diagram* from the Atlantic Ocean outside the coast of Portugal. The joint occurrence for every sea state, specified by the *significant wave height* H_s on the vertical axis and the *peak period* T_p on the horizontal axis, is given in percentage. The shading illustrates the most common sea states, which are centered around an inclined line. The power per meter crest length is given as contours for different power levels. The average power for this site is approximately 54 kW/m and the maximum is 760 kW/m. Furthermore, there are extreme waves and extreme conditions not shown in the scatter diagram. The design criteria for survival for a wave energy plant is usually the 100-year storm wave, which is the highest wave expected at a site over a 100-year period. This power level is much higher than the highest sea state given in Fig. 1.2 and can be up to 100 times the average power.

Harsh environment is another complicating factor. The environment of the oceans is extremely corrosive and all metal structures need to be protected from corrosion . Moreover, depending on where the site is situated the underwater surfaces will be more or less exposed for marine growth. In temperate waters the hard fouling can be over 10 cm thick within some years, which could affect the function of the plant negatively [18].

And finally, access to offshore structures are difficult and costly. Offshore plants needs to be reached by boat and underwater structures may need divers. Boats, and especially divers, need favorable weather conditions to be able to perform maintenance and control, which at good sites (lots of waves) are rare.

1.1.2 Wave energy engineering

We have little means to control the source — the possibilities to influence lies in the engineering. The challenge is to construct a technology that is adapted to the constraints given by the natural resource and that also fulfills the basic

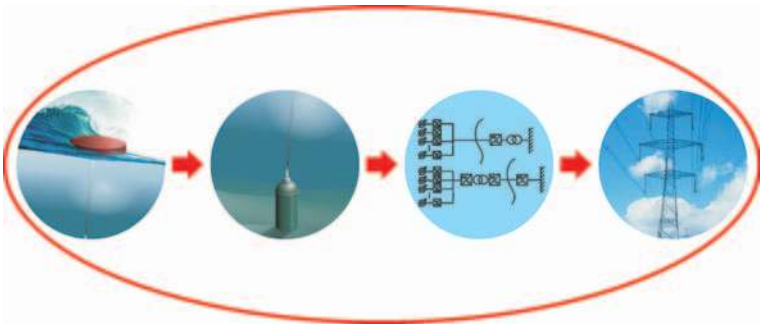

Figure 1.3: Wave energy conversion steps — Absorption, conversion, transmission, and grid connection

demands of profitability and environmental friendliness. Four main issues are highlighted here:

- Survivability — A wave energy plant will be exposed to enormous forces and often there are small possibilities of turning off a wave energy plant. As a consequence, many of the first full scale trials have simply collapsed during storms. This is to a great extent an economical problem. The plant needs to be dimensioned to withstand the forces encountered in a 100–year storm, but will have to be economically viable for much lower average powers.
- Reduced power absorption at higher wave conditions — The ability to reduce the power absorption in larger waves have been identified as one of the crucial questions in wave energy engineering. This is important since it limits the maximum mechanical strains but also the maximum electrical loading. This has impacts on both survivability and on the utility factor.
- Robustness — To be economically viable a wave energy plant needs to be employed for several years and also require a minimum of maintenance. Low maintenance needs are even more important for offshore concepts since access will be difficult and expensive.
- System approach — The conversion of wave energy into electricity fed into a grid consists of four major steps: absorption, conversion, transmission, and grid connection, schematically illustrated in Fig. 1.3. These steps form a very complex system where all parts are intimately linked with each other. It is the performance of the whole system that is the interesting parameter and not the isolated performance of one single component. It is thus very important to have a holistic view and an understanding of the interaction between the different components in the system.

1.1.3 Direct drive vs conventional generators

Most wave energy converter concepts use a conventional high-speed rotational generator to do the conversion from mechanic energy into electric energy. In

order to be able to use a conventional generator, the slow reciprocal motion of the ocean waves needs to be transferred into the fast continuous rotating motion required by the generator. The interfaces needed to perform this conversion tend to increase the complexity of the plant considerably.

In direct drive energy conversion, the generator is adapted to the reciprocal motion of the wave. With a linear generator the motion of the wave can be directly coupled to the moving part of the generator. The mechanical interfaces can then be reduced to a minimum but the generator will need to be larger to compensate for the low speed.

The first attempt to use linear generators in wave energy converters where abandoned [19] and low speed direct drive generators where in early studies ruled out as heavy and inefficient [20]. Progress in permanent magnetic material and power semiconductor devices have, however, opened up for high performance direct drive generators. New wave conversion schemes based on linear generators have been suggested by Mueller [21], and linear generators have been utilized in the offshore testings of the Archimedes Wave Swing [22].

1.2 The wave energy converter concept

The wave energy converter concept, that is the focus of this thesis, uses direct drive technology, but differs from other direct drive concepts in a number of specific ways. The wave energy converter concept is illustrated in Fig. 1.4. A thorough description of the concept can be found in paper VIII and in [23]. A brief description of the concept is given here.

The power absorption is carried out by a floating buoy. This is often referred to as a *point absorber*, which is an absorber that is smaller than half a wave length. The size of the buoy, and thus the whole plant, is naturally limited by the length of the waves. The dynamics of point absorbers have been studied thoroughly by Budal and Falnes, see for example [11, 24] .

The buoy is coupled directly with the moving part, *i.e.* the *actuator*, of a *linear generator*, which is placed on the sea bed. The linear generator is the main subject of this thesis and will be throughly described in the chapters to come. The tension in the rope and the restoring force are provided by a set of springs, which pulls the actuator downwards. The wave crests will pull the buoy and actuator upwards and the springs and mass of the system will drag the actuator and buoy downwards in the wave troughs. The stroke length of the actuator is limited by *end stops* at the top and bottom of the generator that brakes the actuator as it reaches the ends.

Permanent magnets, mounted on the surface of the actuator, will induce a voltage when they move in relation to the *stator*. This will drive a current in the cable windings in the stator. Since the actuator speed is varying, both the frequency and amplitude of the induced currents will vary and cannot be di-

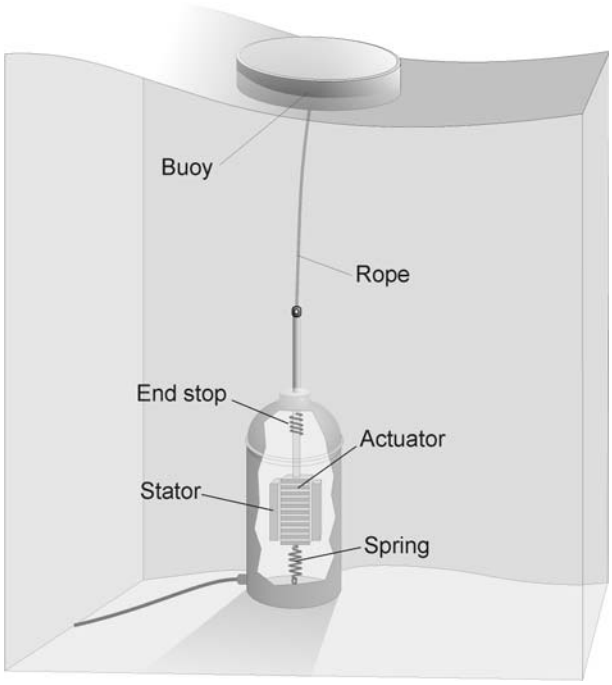

Figure 1.4: Illustration of wave energy converter unit

rectly connected to a AC-grid. The current of a generator is therefore rectified and the DC-current from several units are interconnected. The power is transmitted ashore through sub-sea cable. A converter converts the DC-current into AC-current and feeds it to the grid. The DC–AC converter can be placed either offshore or onshore depending on the the total power of the plant [25].

1.3 Aim of thesis

This work is a part of a larger project carried out at Uppsala University, which aims to investigate and develop the wave energy converter concept introduced above. The focus of this thesis lies on the conversion step and on the linear generator of the wave energy converter. The research on the conversion step is carried out in parallel with research on the hydrodynamic behavior of the plant, i.e. the power absorption [26, 27, 28], and research on the transmission and grid connection [29, 30, 25].

The thesis is based on a number of papers, which describe the research work from the first simulations and design studies, via a laboratory prototype, to the first full scale offshore testing of a wave energy converter. Although the focus of this thesis is on the linear generator, system approach permeates the work and the superior aim is always to optimize the whole system. This is reflected

in some of the papers, which studies the wave energy converter as a concept and its behavior in different waves.

The introduction stresses the necessity of finding and exploiting new energy sources and aims to give an unbiased insight into wave energy conversion.

The aim of the theory section is to give the basis for electromechanic energy conversion and to derive analytical expressions necessary to understand the basic mechanisms in permanent magnetized linear generators. The analytical theory is also adapted for these new types of variable speed machines and 'synchronous inductance' is utilized instead of the classic 'synchronous reactance'. The description of the numerical method focuses on the different models adopted in the calculation, but does not consider numerical methods involved in the solving of the finite element problem. The derivation of the longitudinal end effect model is comprised as a whole. This is the first analytical model that describes the flux distribution in a linear machine, taking the longitudinal ends into account. The final expression for the flux is used in chapter 7 and in paper V.

The theory is followed by an introduction to linear machines, where the basic conditions for linear generators in wave energy conversion and a description of the specific machine type, are given.

The following chapters summarize and discuss the results presented in the papers. They are followed by a discussion, where some of the more important results are highlighted and discussed. Finally, a summary of the most important conclusions of the thesis is given, followed by a summary of the papers that describe how the papers are related and the contribution of the author.

The goal is that the thesis should be comprehensible also to people who are not particularly familiar with electric machine theory. It is however unavoidable that some parts are rather technical.

2. Theory

Although electric machines at a first glance are very simple — the basic principles can easily be illustrated for child groups by moving a magnet in and out of a coil and make small lamp to flash — a deep theoretical description can be very complex. The electromechanical energy conversion involves magnetization processes on nano-scale up to interaction with national electricity grids. To be able to model such a system, we need to implement a number of simplified models where the main characteristics of different phenomena is interpreted by a finite set of parameters.

There exists today a wide range of different models. They can briefly be divided into more simple circuit models and more complex field models. The simple analytic models have the advantage of being fast and have a pedagogic value since they provide simple relations between different entities in the electric machines. More complex field models give more accurate modeling but takes longer time to compute and some of the intuitive understanding is somewhat eclipsed.

The first part of this chapter has a pedagogic ambition. It starts with an introduction to the principles for electromagnetic energy conversion, which is followed by a derivation of the basic equations for the generator investigated in this thesis. The theory is based on traditional electric machine theory, but goes deeper into some of the more physical aspects of electromagnetic machines. The aim of this part is not to give a complete theory for electric machines but to give a general understanding of the electromechanical energy conversion and the basic principles of the generator investigated in this thesis. This is followed by a description of the FE-based numerical model used throughout this work. The chapter ends with the derivation of an analytical model developed to investigate the influence of longitudinal ends.

2.1 Electromechanical energy conversion

Electric generators are utilized to convert mechanic energy into electric energy. If losses are ignored the process is reversible and in principle all generators can function in motor mode, where electric energy is converted into mechanic energy. The fundamental equation for a conversion process, defined in generator mode is:

$$\Delta W_{mechanic} = \Delta W_{electric} + \Delta W_{field} + \Delta W_{loss} \tag{2.1}$$

where $\Delta W_{mechanic}$ is the mechanic energy supplied to the system, $\Delta W_{electric}$ is the electric energy extracted from the system, ΔW_{field} is the energy associated with the magnetic field, and ΔW_{loss} is the thermal energy produced in loss processes. The magnetic field energy term W_{field} varies over time but does not represent a net consumption of energy. It plays however an important role in the generator since the magnetic field acts as the coupling media between the mechanic and electric systems.

In power applications, electromechanical energy conversion is based on the interaction between magnetic fields, current carrying conductors, and ferromagnetic material. When a conductor is moving relative to a magnetic field, or a coil is experiencing a changing magnetic flux, an *electromotive force* (emf), E, will be induced in the conductor or coil. This this is known, for the coil case, as the *Faraday's law of induction*:

$$E = -\frac{d\phi}{dt}, \tag{2.2}$$

where ϕ is the magnetic flux enclosed by the coil. If the conductor forms a closed loop, the emf will drive an electric current through the conductor. Faraday's law of induction thus explains how movement of a magnetic field can be used to induce electricity. This is just half the truth since we also need a force working in opposite direction to the motion to explain the mechanic energy input. The mechanical interaction between current carrying conductors was initially described by Ampere. This interaction was attributed to a vector field, which is the today well established *magnetic induction field* $\mathbf{B}$. *Ampere's circuital law* relates the magnetic induction field to its source, the current density, J, as follows:

$$\oint \mathbf{B} d\mathbf{l} = \mu_0 I_{enc}, \tag{2.3}$$

where I_{enc} is the current enclosed by the integration, and μ_0 is the permeability of vacuum. With this definition of $\mathbf{B}$ the force on the conductor will be expressed as follows:

$$F = I \oint_C d\mathbf{l} \times \mathbf{B}(x). \tag{2.4}$$

The mechanical interaction between the different parts of the generator can be viewed in terms of (2.3) and (2.4), where permanent magnet also can be interpreted as current carrying coils. In reality, the ferromagnetic steel in the generator plays an important role and a lot of the mechanical interaction is actually transferred to these parts.

2.2 Linear permanent magnet synchronous generator

The mode of function can vary considerably between different generators but the theory will here be restricted to linear synchronous generators with permanent magnet excited flux. The generator consist of a moving part and a static

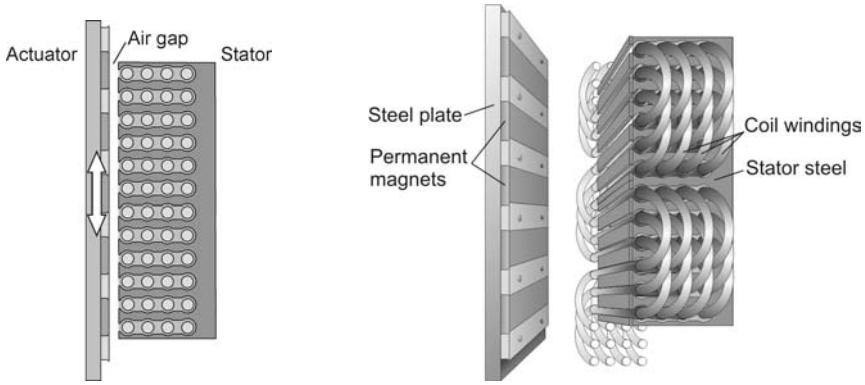

(a) Side view of linear generator (b) Cutaway view of linear generator

Figure 2.1: Illustration of a linear synchronous generator

part, see Fig. 2.1. The moving part, here referred to as the *actuator*[1], moves in a reciprocal linear motion and consists of a ferromagnetic steel plate with surface mounted permanent magnet. The static part is called the *stator* and consists of three phase coil windings wounded around a laminated ferromagnetic iron core. Between the actuator and the stator is a physical distance called the *air gap*, which allows the relative motion of the two parts. The air gap does not necessarily need to be air, but could be other media that allows motion and that does not interfere with the magnetic field, *e.g.* water. Strong attractive forces are apparent between the actuator and the stator and a supporting structure is required to hold the actuator and stator in place. The supporting structure is not illustrated in Fig. 2.1, but will be discussed in chapter 5 and 6. The generator will be described more thoroughly in section 3.4.

2.2.1 Lumped circuit of synchronous generator

A simple linear lumped circuit can often be useful to describe main electric characteristics of the generator. However, it should be noted that this is a rough model and its merits are mostly pedagogical. The generated voltages and currents of the generator will be described in a general manner were the fluxes, voltages, and currents are assumed to have sinusoidal space and time variation. The notation will refer the peak values of the time varying entities. Furthermore, non-linear effects are at this stage neglected and different flux waves are supposed to be superpositionable.

The lumped circuit diagram of one phase of a synchronous generator is illustrated in Fig. 2.2. One phase of the generator is modeled by an emf, a

[1]The moving part is traditionally referred to as the 'rotor' due to the rotational motion in rotating machines. This is not suitable for a linear machine where the motion is linear. However, there is no real consensus in the nomenclature and the actuator can also be referred to as *alternator*, *mover* and *piston*.

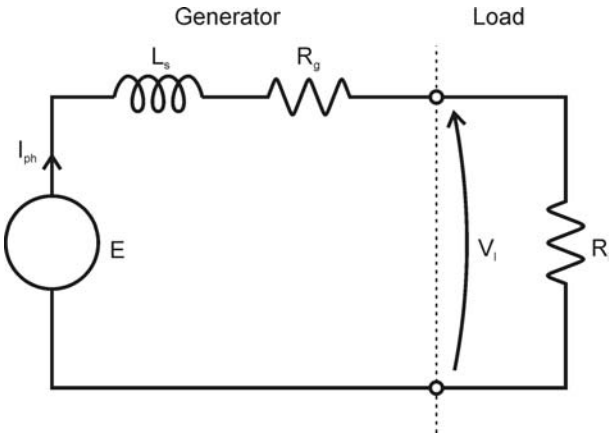

Figure 2.2: Lumped circuit diagram of one phase of a synchronous generator

resistance, an inductance, and a load. The emf, E, is the voltage induced by the permanent magnet flux wave. This voltage is also called the *no-load voltage* since it is the voltage that will be measured over the phase connections if no load is connected. Inside the generator there are a resistive voltage drop, due to the winding resistance, R_g, and an inductive voltage drop modeled by the synchronous inductance, L_s. The load, R_l, is here modeled as a purely resistive load[2].

Since the no-load voltage is assumed to vary sinusoidally and all components have a linear behavior the $j\omega$-method can be used. From the lumped circuit we can determine, among other things, the *load voltage*:

$$V_l = \frac{ER_l}{R_l + R_g + j\omega L_s}, \tag{2.5}$$

the *phase current*:

$$I_{ph} = \frac{E}{R_l + R_g + j\omega L_s}, \tag{2.6}$$

and the power in the load:

$$P_l = \frac{E^2 R_l}{(R_l + R_g)^2 + (\omega L_s)^2}. \tag{2.7}$$

To estimate the main characteristics of a synchronous generator with resistive load it suffices to know the parameters: E, L_s, R_g, and R_l. The induced emf E and the synchronous inductance L_s will be explained in the following sections.

[2]In reality the current of the generator will be rectified and connected to a DC-bus. A rectification bridge is a non-linear component and cannot be modeled with linear circuit theory. A resistive load, however, resembles a passive rectification bridge by having a power factor equal to one, *i.e.* the voltage and the current is in phase.

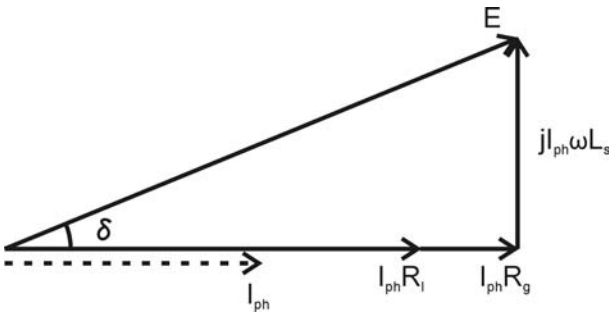

Figure 2.3: Phasor diagram of a synchronous generator with resistive load

The relation between the different voltage components in the lumped circuit can be illustrated by phasor diagram, see Fig. 2.3. The phase of the current is indicated with a dashed arrow. Resistive voltage components are in phase with the phase current and inductive voltage components are phase shifted $\pi/2$ electric degrees before the phase current.

The angle, δ, between the emf, E, and the load voltage, V_l, is called the *load angle*, and is in a machine with resistive load a measure of the inductive voltage drop in the machine. From the phasor diagram, we see that the load angle can be expressed in terms of the synchronous inductance, the frequency, the winding resistance, and the load resistance, as follows:

$$\delta = \arctan\left(\frac{\omega L_s}{R_l + R_g}\right). \tag{2.8}$$

or in terms of the induced emf, the synchronous inductance, the phase current, I_{ph}, and the frequency:

$$\delta = \arcsin\left(\frac{I_{ph}\omega L_s}{E}\right). \tag{2.9}$$

2.2.2 Induced emf

The permanent magnets are mounted with alternating polarity, which will create a magnetic flux wave with alternating direction. This flux is the *permanent magnet flux* of the machine and the flux wave will follow the actuator as it moves. In Fig. 2.4 the permanent magnet flux and the coil windings of one phase are illustrated. The flux passing through one coil, shaded in the figure, will be a function of the actuator position, x'. When the actuator moves relative to the stator, the stator coils will experience a changing magnetic flux and, according to (2.2), an emf will be induced in the coils. If we take the most simple case, we can assume that the flux wave has a sinusoidal distribution and that the width of the coils, w_{coil}, are equal to the pole width w_{pole}. The total induced emf will then vary sinusoidally and the amplitude can be expressed

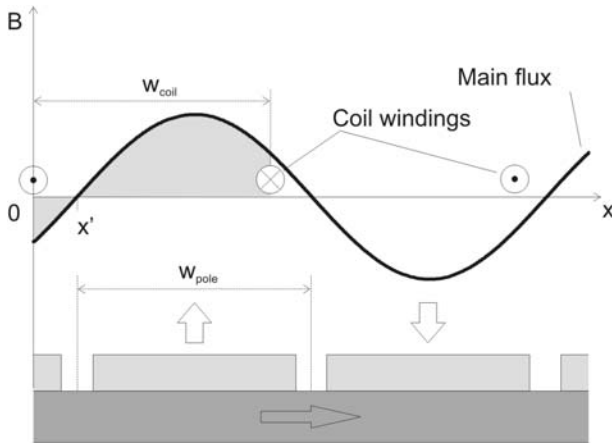

Figure 2.4: Permanent magnet flux wave in air gap. The integration of the flux over one coil width is shaded.

as follows:

$$E = \omega \phi_{pm} N_{pole} N_{turns}, \tag{2.10}$$

where N_{pole} is the total number of poles, N_{turns} is the number of coil turns per pole, ϕ_{pm} is the permanent magnet induced flux per pole, and ω is the angular frequency. This is the 'classic' expression, which gives the induced voltage as a function of frequency. We can rewrite this expression by using the relations: $\omega = 2\pi v / w_{pole}$, and $\phi = l_{stack} w_{pole} B_{pm} 2/\pi$, where v is the actuator speed, l_{stack} is the stack length of the stator, *i.e.* the width of the stator, w_{pole} is the pole width, and B_{pm} is the amplitude of the permanent magnet induction. We will then get the induced emf as a function of actuator speed:

$$E = 2 B_{pm} N_{pole} N_{turns} l_{stack} v. \tag{2.11}$$

The induced voltage will thus depend on the strength of the magnetic field, the total number of coil turns, the stack length, and the speed of the actuator. In reality there is a lower limit of the pole width and we see that, for a fix pole width, $N_{pole} l_{stack} \propto A_{air}$. The induced emf will then be proportional to the air gap area, the magnetic induction, the number of turns per coil, and the speed:

$$E \propto A_{air} B_{pm} N_{turns} v. \tag{2.12}$$

2.2.3 Synchronous inductance

The amount of flux that a circuit, c, creates, that is coupled with another circuit, b, can be expressed in terms of the current in the first circuit I_a and the *mutual inductance* $L_{a,b}$ between the circuits, as follows:

$$\Phi_{a,b} = L_{a,b} I_a, \tag{2.13}$$

where $\Phi_{a,b}$ is circuit b's *flux linkage* with the flux induced by circuit a.

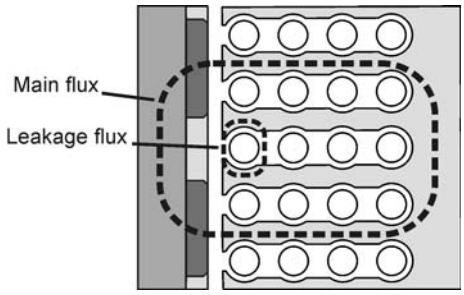

Figure 2.5: Main flux and leakage flux in the magnetic circuit.

The field produced by the phase currents can be divided into two components, one component which is coupled with the entire magnetic circuit, *i.e.* the *main flux*, and the other component is leakage flux This is illustrated in Fig. 2.5. The corresponding inductances are defined as the *main inductance*[3], L_m, and the *leakage inductance*, L_l, respectively.

The inductance of a coil is proportional to the square of the number of coil turns divided by the reluctance of the magnetic circuit. The main inductance of the generator can thus be expressed:

$$L_m \propto \frac{N_{pole} N_{turns}^2}{\Re}. \tag{2.14}$$

The synchronous inductance in the lumped circuit models the phase winding's total flux linkage with the flux induced by all three phase currents. In a symmetric system the synchronous inductance can be expressed in terms of main inductance and leakage inductance, as follows:

$$L_s = \frac{3}{2} L_m + L_l, \tag{2.15}$$

where the first term is the *armature flux* linkage with the phase winding, which will be described below, and the second term is leakage inductance of that phase.

In traditional generator theory it is common to define a *synchronous reactance* for the machine, which is simply the synchronous inductance multiplied with the frequency $X_s = \omega L_s$. This is however inconvenient for a machine where the frequency is varying continuously.

2.2.4 Armature flux

To understand the forces in a generator one needs to study the magnetic fields. The forces are a result of the interaction between the permanent magnet flux,

[3]The inductances for the permanent magnet linkage and phase winding linkage with the armature flux are proportional, but not identical. This have no implication on the the theoretical descriptions here and they will both be referred to as main inductance.

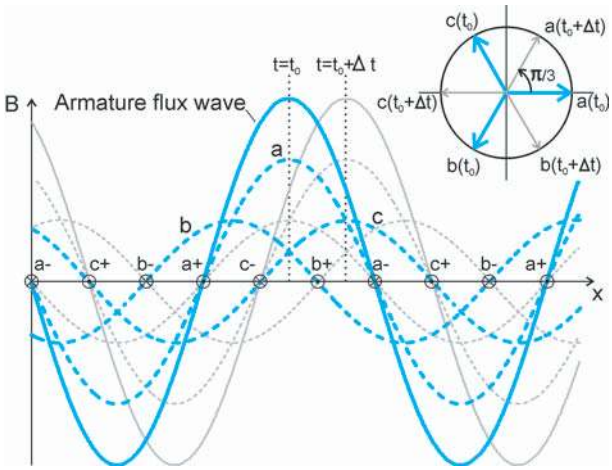

Figure 2.6: The flux waves from the three phases (a,b, and c) at a time t_0 and the resulting armature flux wave. The fluxes for a time $t = t_0 + \Delta t$ are illustrated in gray lines.

which follows the actuator, and the *armature flux*, which is the flux created by the stator currents.

The generator has three individual coil circuits, *i.e. phases*. The centers of the different phases are geometrically shifted $2/3$ pole widths in the direction of motion. If a symmetric load is connected to the generator, the three phases will each carry a phase current, individually shifted $2\pi/3$ electrical radians. The current of one phase will give rise to a pulsating magnetic field, which is stationary relative to the stator. However, the superposition of the magnetic field from all three phases will give rise to a resulting flux, the armature flux, which will be moving with the actuator. This is illustrated in Fig. 2.6 where the flux contribution of all three phases and the resulting armature flux are given at a time $t = t_0$.

The phasor diagram, in the right upper corner, illustrates the phases of the fluxes as a function of time. At time $t = t_0$, the flux of phase a will be at maximum and the fluxes of phases b and c will have negative sign and half the amplitude of phase a. Due to the geometrical displacement the fluxes from phases b and c will give a positive contribution at the center of phase a. At time $t = t_0 + \Delta t$, where the pointers have turned $\pi/3$ radians, the phase c will have negative maximum and phase a and b will be positive and half the maximum amplitude. The armature field will then have moved $\pi/3$ to the right, which is illustrated with thin gray lines.

The amplitude of the phase flux linkage with the permanent magnets $\Phi_{ph,pm}$ is given by the stator current amplitude I_{ph} and the main inductance L_m:

$$\Phi_{ph,pm} = L_m I_{ph}. \tag{2.16}$$

From the figure, we see that the amplitude of the magnetic induction of the armature flux wave, B_a, in terms of the amplitude of the magnetic induction

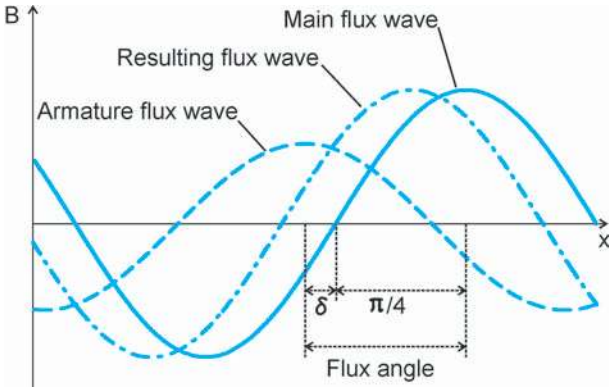

Figure 2.7: Permanent magnet flux wave, armature flux wave, and resulting flux wave in air gap. The fields are moving to the right in the figure.

of the phase fluxes B_{ph} will be:

$$B_a = \frac{3}{2} B_{ph}. \tag{2.17}$$

The armature flux linkage with the permanent magnets can thus be expressed in terms of main inductance L_m and the stator current amplitude I_{ph} as follows:

$$\Phi_a = \frac{3}{2} L_m I_{ph}. \tag{2.18}$$

The permanent magnet flux wave, the armature flux wave, and the resulting flux wave are illustrated in Fig. 2.7. The flux waves are here regarded as waves with constant shape that is moving in time to the right in the figure. The phase shift between the permanent magnet flux and the armature flux can be understood by studying the phasor diagram in Fig. 2.3. The permanent magnet flux wave will precede the induced emf by an angle of $\pi/2$ radians. The armature flux, in turn, will be in phase with the armature current. The armature flux wave will thus lag the permanent magnet flux wave by an angle $\pi/2 + \delta$.

In generator mode the permanent magnet field precedes the armature field. The force between two magnetic field acts in the direction so that the fields will be aligned. The components creating the permanent magnet field will thus experience a force acting toward the the armature field, which is opposite the direction of motion. This is the *damping force* of the generator. Similarly, the components creating the armature field will experience a force in the other direction.

The air gap force, F_g, will be at maximum if the fields have an internal displacement of $\pi/2$. This is not possible for a machine with resistive load, since this would imply $\delta = 0$, and we would have no armature flux. However, the forces between the fields decreases as the angle between the fields increases. It can be shown that for a machine with resistive load:

$$F_g \propto B_m B_a \cos(\delta). \tag{2.19}$$

It is stressed that load angle and armature flux are linked.

2.3 Maxwell's equations

The electromagnetic field theory is summarized in the famous *Maxwell's equations*:

$$\nabla \cdot \mathbf{D} = \rho_f \tag{2.20}$$

$$\nabla \times \mathbf{E} = -\frac{\partial \mathbf{B}}{\partial t} \tag{2.21}$$

$$\nabla \cdot \mathbf{B} = 0 \tag{2.22}$$

$$\nabla \times \mathbf{H} = \mathbf{J}_f + \frac{\partial \mathbf{D}}{\partial t} \tag{2.23}$$

Maxwell's equations relates vector fields, electric current densities, and electric charge densities. The vector fields are the *electric displacement field* **D**, the *electric field* **E**, the magnetic induction **B**, and the *magnetic field strength* (or simply the *magnetic field*) **H**. The current density $\mathbf{J}_f$ is the *free current density* and the charge density ρ_f is the *free charge density*.

The first equation (2.21) relates the electric displacement field with the free charge distribution. The second equation (2.21) can be recognized as the vector formula for Faraday's law of induction (2.2). The third equation (2.22) states that the flux through a closed surface is equal to zero, which for a two dimensional flux means that the flux lines forms closed paths. The fourth equation states that the curl of the magnetic field strength **H**, is equal to the sum of the free current density and the time derivative of the displacement field. This is a more general version of equation (2.3). The free current can be related to the electric field in linear conducting media by the conductivity σ:

$$\mathbf{J}_f = \sigma \mathbf{E}. \tag{2.24}$$

This is equivalent to the *Ohm's law* for macroscopic conductors.

For a complete theory, this set of equation needs to be supplement with equations that relates the electric field intensity **E** with the electric displacement field **D** and the magnetic induction **B** with the magnetic field **H**. The latter will be clarified when the presence of magnetic materials are introduced in the next section.

2.4 Magnetic materials

The magnetic field, as defined in (2.23), only considers the free current density and the time derivative of the displacement field. The free current densities

are currents, which we can control, such as currents in conductors, electron beams, etc. There are however more sources to the magnetic induction and that is the current associated with the constituents of matter.

The electrons moving around the nucleus or spinning around its own axis can be interpreted as a current loop and according to (2.3) they will induce a magnetic field. The microscopic magnetic dipole moment, created by bounded electron motion, can in some cases give a resultant macroscopic magnetic dipole moment different from zero. The material is then said to be *magnetized* and the resulting field from the intrinsic dipoles is the *magnetization field* $\mathbf{M}$. This field is attributed to the *magnetization current density* $\mathbf{J}_m$, which differs from the free current density $\mathbf{J}_f$ since it is a current corresponding to the bound electrons moving around the atom nuclei. The magnetization field is related to the magnetization current density as follows:

$$\mathbf{J}_m = \nabla \times \mathbf{M}, \tag{2.25}$$

which can be compared with the last of Maxwell's equations (2.23). The magnetic induction $\mathbf{B}$ is the resulting field from all currents and is the sum of the magnetization field $\mathbf{M}$ and the magnetic field $\mathbf{H}$ multiplied with the permeability of free space μ_0:

$$\mathbf{B} = \mu_0 (\mathbf{M} + \mathbf{H}). \tag{2.26}$$

This equation is the equation that we asked for in the previous chapter, which relates the magnetic induction with the magnetic field. If the magnetization is assumed to be proportional and parallel to the applied magnetic field the magnetization can be expressed as

$$\mathbf{M} = \chi_m \mathbf{H}, \tag{2.27}$$

where χ_m is the *magnetic susceptibility* of the material. Often the relation between the magnetic field and the magnetic induction is written on the form:

$$\mathbf{B} = \mu_r \mu_0 \mathbf{H}, \tag{2.28}$$

where

$$\mu_r = 1 + \chi_m. \tag{2.29}$$

Here μ_r is the *relative permeability* of the material. This notation is frequently used even for materials where the magnetization has a very complex relation to the magnetic field and it should be noted that the relative permeability then is a function of several parameters.

The most important materials for power applications are the ferromagnetic materials. Significant for the ferromagnetic materials is the high relative permeability and the non-linear behavior of the magnetization. The magnetization in a ferromagnetic material depends on a number of factors, such as applied magnetic field, magnetic history, temperature, etc. A typical magnetization curve of a ferromagnetic material is shown in Fig. 2.8. This figure show

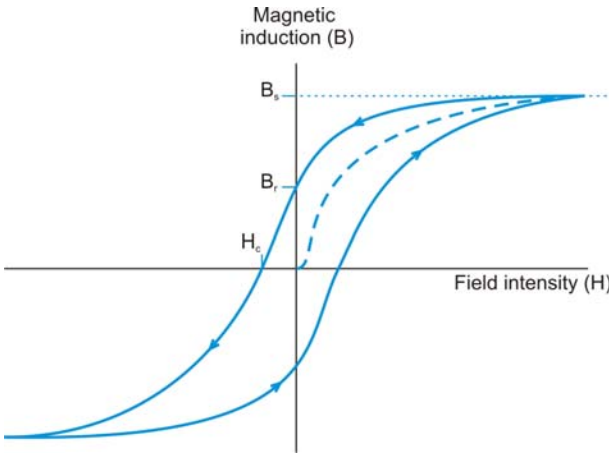

Figure 2.8: Characteristic BH-curve of a ferromagnetic material. The initial magnetization curve is the dashed line starting from origo.

the resulting magnetic induction, **B**, as a function of the applied magnetic field, **H**. The dashed line represents the *initial magnetization curve*, which is the magnetization characteristics of a demagnetized material. The magnetic induction increases rapidly at the beginning as the magnetic field is increased but levels off as the magnetic induction reaches a certain level. The magnetization of the ferromagnetic material has reached the *saturation* level and the corresponding magnetic induction is the *saturation magnetic induction* B_s. When the magnetic field is decreased the magnetic induction will follow a new curve slightly higher than the initial magnetization curve. This is due to hysteresis of the magnetization. When the magnetic field is reduced to zero the material will still be magnetized and the resulting magnetic induction is called *remenance magnetic induction* B_r. The magnetic field necessary to get zero magnetic induction is called the *coercive field*, H_c. If a ferromagnetic material is subjected to a fluctuating magnetic field, the BH-characteristic will follow a *hysteresis loop*, which is the the solid curve in Fig. 2.8.

The relative permeability of a ferromagnetic material varies considerably for different levels of magnetization, which is illustrated in Fig. 2.9. When the magnetic induction reaches saturation level, the permeability drops fast, and highly saturated materials will have permeabilities close to air.

The magnetization characteristics of a ferromagnetic material depends also on the temperature. Thermal motion in the material counteracts the alignment of the magnetic dipoles and the susceptibility is decreasing with increased temperature. If the temperature exceeds a certain temperature the dipole will no longer align and the material ceases to be ferromagnetic. This is called the *Curie temperature*.

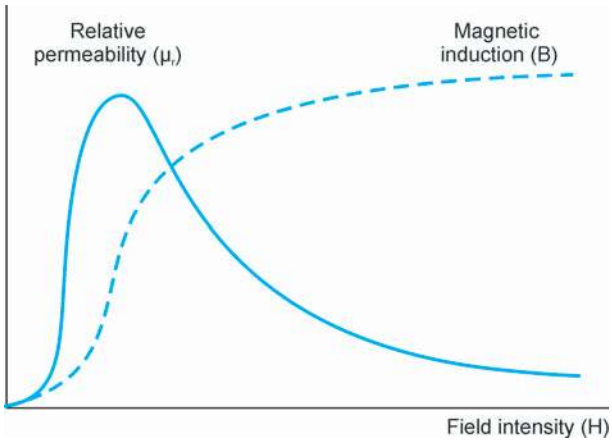

Figure 2.9: Relative permeability and magnetic induction of a ferromagnetic material as a function of magnetic field.

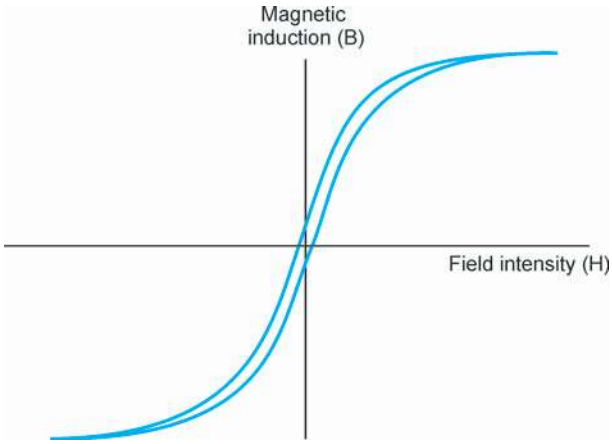

Figure 2.10: BH-curve of soft ferromagnetic material.

2.4.1 Soft ferromagnetic materials

The magnetic materials used in generators are *soft ferromagnetic materials* and *permanent magnet material*. The soft magnetic material serves as conductor of the magnetic flux and is characterized by high relative permeability, high magnetic saturation induction, low remanence magnetic induction, and low coercive field strength. A typical BH-curve of a soft ferromagnetic steel is illustrated in Fig. 2.10. Low remanence magnetic induction and low coercive field strength reduces the the hysteresis losses. Often the conductivity of the material is reduced in order to minimize the influence of eddy current losses. Losses associated with the soft magnetic steel will be further discussed in section 2.5.

2.4.2 Permanent magnet material

Permanent magnet are characterized with high remenance magnet induction and high coercive field strength. The BH-curve and the MH-curve of a permanent magnet is illustrated in Fig. 2.11. The MH-curve gives the magnetization as a function of the magnetic field and can be derived from the BH-curve using (2.26).

Under normal working condition a permanent magnet will be subjected to a negative magnetic field and the working point of a permanent magnet will move along the BH-curve and MH-curve in the second quadrant, as illustrated in the figure. This part is called the *demagnetization curve* of the permanent magnet and the linear part can be modeled as follows:

$$\mathbf{B} = B_r + \mu_{rec}\mu_0\mathbf{H}, \tag{2.30}$$

where B_r is the remanence magnetic induction and μ_{rec} is the *recoil permeability*, which corresponds to the slope of the BH-curve.

As can be seen, the magnetization is almost constant in the working area, however, the magnetization of the permanent magnet will change drastically if the negative magnetic field exceeds the *intrinsic coercive field* H_{ic}. If the negative magnetic field exceeds the intrinsic coercive field the magnet will be *de-magnetized* and permanently damaged. As long as the negative magnetic field is smaller than the intrinsic coercive field the magnetization is fully recoverable.

The energy of the magnetic flux produced by a permanent magnet is proportional to the product of the magnetic field and the magnetic induction. The maximum magnetic energy in the second quadrant is the *maximum energy product*, which is used as figure of merit, as it gives a measure of how large magnet volume that is needed for a certain flux. The intrinsic coercive field is temperature dependent and decreases with increasing temperature. High temperature will both decrease the maximum energy product of the magnet and increase the risk of de-magnetization.

2.5 Losses

The losses can be divided into three parts, namely: losses in the conductors, *i.e. copper losses*, losses associated with the magnetic field, *i.e. eddy current losses*, *hysteresis losses* and *excess losses*, and finally mechanical losses.

2.5.1 Copper losses

The losses in the conductors consists of resistive losses and an additional term, which is attributed to the magnetic field in the conductor. The resistive loss

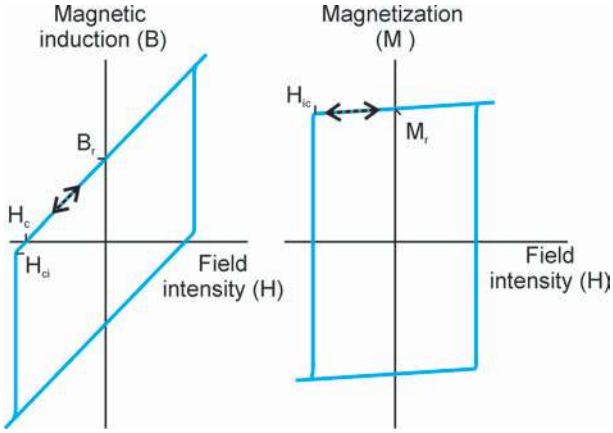

Figure 2.11: BH-curve and MH-curve of a permanent magnet. The working point under normal conditions is marked with a dashed black arrow.

density, or *ohmic loss* density, is given by:

$$p_{ohm} = \mathbf{J}_f \cdot \mathbf{E} = \sigma \mathbf{E}^2 = \frac{\mathbf{J}_f^2}{\sigma}, \tag{2.31}$$

where the last two equalities are given by using (2.24). For a macroscopic conductor this can be rewritten in terms of total current, J, voltage drop over the conductor, V, and total resistance of the conductor, R:

$$P_{ohm} = JV = J^2 R = \frac{V^2}{R}, \tag{2.32}$$

where the macroscopic version of (2.24), $J = V/R$, have been used. The resistance of a conductor depends on the cross section area, A_c, the length, l_c, and the conductivity σ:

$$R = \frac{l_c}{A_c \sigma}. \tag{2.33}$$

This assumes a homogeneous current distribution in the conductor. A conductor with varying current will however have non-homogeneous magnetic field inside the conductor, which will give a non-homogeneous current distribution. This is known as *displacement current* and will increase the apparent resistance of the conductor and thus the losses. This effect is however negligible at the frequency range of this application.

2.5.2 Eddy currents

Eddy currents are found in any conductive media that is subjected to a time-varying magnetic field. These current will give rise to heat through ohmic losses, reaction fields, and forces resulting from the interaction of the inducing and the reaction field.

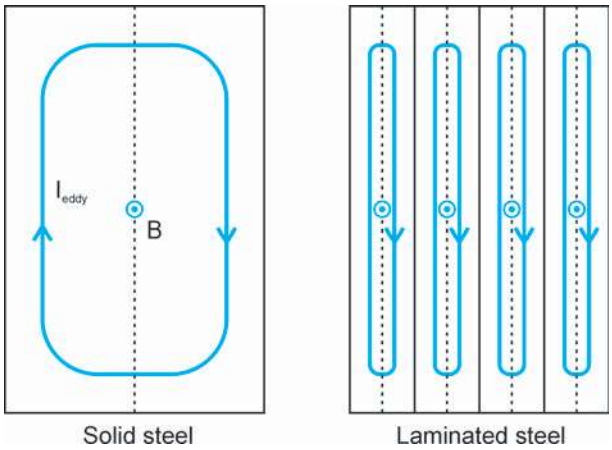

Figure 2.12: Eddy currents in solid and laminated steel. The direction of the magnetic intensity is perpendicular to the plane.

The amplitude of the eddy currents depends on the time derivative of the magnetic induction, the area of the current loop, and the resistance experienced by the current. Eddy currents will thus be large in the steel parts of the generator where the magnetic induction is varying much, *i.e.* the stator. The eddy currents are reduced by using laminated, electrically isolated sheets in the stator. This forces the eddy currents into narrow rectangular loops, where the quota between the area and the resistance is much smaller than for a solid material. This is illustrated in Fig. 2.12, which show the eddy currents in a solid steel and in laminated steel.

The eddy currents in laminated materials are said to be *resistance limited eddy currents*, and the reaction field produced by the them is small. This is desirable in the stator, since a high reaction field will give reduced permanent magnet flux. The eddy current loss density in laminated materials can be approximated as:

$$p_{eddy} = \frac{d_l^2 \omega^2 B_{rms}^2 \sigma}{12}. \tag{2.34}$$

where σ is the conductivity of the steel, ω is the angular frequency of the field, and B_{rms} is the root mean square value of the magnetic induction.

In solid materials, however, the reaction field can be significant and the eddy currents are then *inductance limited*. The eddy currents will be resistance limited as long as the lamination is thinner than half the *skin depth* δ_s, which can be calculated from conductivity σ, frequency ω, and relative permeability μ_r [31]:

$$\delta_s = \sqrt{\frac{2}{\omega \sigma \mu_0 \mu_r}}. \tag{2.35}$$

2.5.3 Hysteresis losses

The magnetization process in steel is a complex process, which is characterized by the modulation of *magnetic domains*. Magnetic domains are small volumes were the magnetic dipoles are aligned. When an external field is applied the magnetic domains undergo a number of modulations. Most of these processes are reversible, however some are irreversible and give rise to hysteresis in the magnetization, *i.e.* the magnetization will not return to original state when the applied magnetic field is reduced. The hysteresis is illustrated in Fig. 2.8 and the power loss for one period is given by the area encircled by the BH-curve. The irreversible processes increases as the magnetization increases and the area of the hysteresis curve can be approximated as being proportional to the square of the maximum magnetic intensity B_{max}. The fundamental angular frequency determines the rate of cycles per time and the hysteresis losses density can be modeled as follows:

$$p_{hysteres} = k_h B_{max}^2 \omega, \tag{2.36}$$

where k_h is a material constant and f is the fundamental frequency.

2.5.4 Excess losses

Excess losses are the difference between the losses predicted by (2.34) and the measured losses. The origin of the excess losses are not completely understood, but the excess loss density can be approximated by [32]:

$$p_{excess} = k_e \left(B_{max}\omega\right)^{3/2}, \tag{2.37}$$

where k_e is a material parameter that can be obtained from experiments.

2.6 Influence of non-linearities in electric machines

In the electric machine theory above we assumed that the magnetic field components from different sources could be regarded as separate fields and that they could be superimposed linearly into a resulting field. Furthermore, the components in the lumped circuit were assumed to be constant.

The non-linear magnetization of the steel parts, however, influence the magnetic field considerably. Especially, when the magnetization is near saturation, the resulting field will differ from the sum of the separate fields. If the fields interact positively, the resulting field will be lower then the sum of the two separate field components due to the increasing saturation, and the contrary, if the fields counteract each other the resulting field will be larger due to decreasing saturation.

Since the properties of the steel will change as the magnetic fields varies, the parameters, which depends on the the magnetic steel, will vary as well.

Consequently, the induced emf, E, as well as the synchronous inductance, L_s, will depend on the phase currents.

Other non-linear phenomena are eddy currents and hysteresis. Eddy currents creates reaction fields, whose amplitude depend on the frequency of the magnetic field. The apparent permeability of the steel will thus vary with the frequency.

2.7 Finite element modeling

Finite element (FE) modeling is a mathematical method where partial differential equations (field equations) are solved for a geometry subdivided into nodes. Today there exists a well established frame work of modeling of electric machines by FE-modeling. Steady state, as well as transient problems can be solved, where geometry, non-linear material properties, external circuits are taken into account. The major limitation for FE-method based modeling is the considerable computational effort that is needed. A lot of effort has been made to develop methods that reduces the computational effort. However, these methods often imply simplifying assumptions and should be used with care.

2.7.1 Field formulation

From the Maxwell's equations it is possible to derive an expression [33]:

$$\nabla \times \left(\frac{1}{\mu_r \mu_0} \nabla \times \mathbf{A} \right) + \sigma \frac{\partial \mathbf{A}}{\partial t} = \mathbf{J}_0, \tag{2.38}$$

which solves the electromagnetic equations for the vector potential, $\mathbf{A}$, which is given by:

$$\mathbf{B} = \nabla \times \mathbf{A}. \tag{2.39}$$

The second term on the left hand side in (2.38) represents the *induced currents* and the right hand term, $\mathbf{J}_0$, gives the *applied currents*. To arrive to this expression we have neglected the displacement current term $\partial \mathbf{D}/\partial t$ in (2.23), which is possible for low frequency application.

To simplify further we assume that the magnetic flux is two-dimensional [34]. The flux will then be assumed to be symmetric along the z-axis, as defined in Fig. 2.13, and the vector potential will be reduced to the scalar $\mathbf{A} = A_z$. Such an approach is possible if the width of the machine is significantly larger than the air gap width [35]. However, all stray fluxes outside the machine will be neglected. We can then simplify the above expression as follows:

$$\nabla \cdot \left(\frac{1}{\mu_r \mu_0} \nabla A_z \right) + \sigma \frac{\partial A_z}{\partial t} = J_s + J_{pm}. \tag{2.40}$$

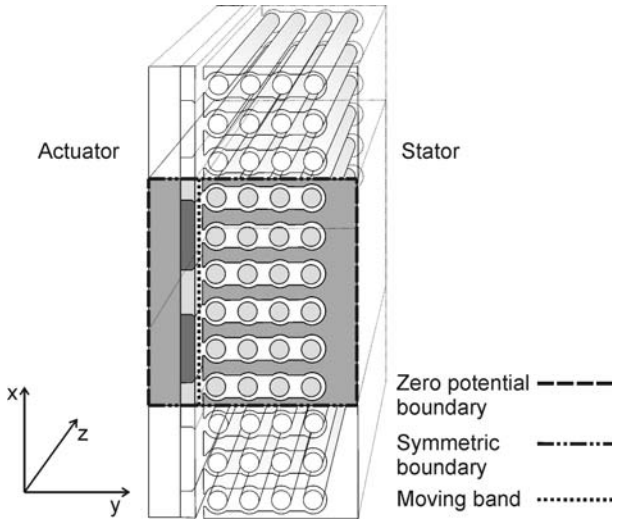

Figure 2.13: Two-dimensional computational domain and boundary conditions.

The right hand side, which represents the applied currents, are now subdivided into J_s, which models the current densities in the stator windings, and J_{pm}, which models the coercive field in the permanent magnets, see section 2.7.3.

The finite element solution models are solved together with the electric circuit equations. The electric circuit equations model the winding resistance, coil-end inductances, and the load. This results in a coupled field and circuit model, which is solved simultaneously [36].

2.7.2 Cyclic boundary condition and internal moving boundary

Rotating generators have a physical and electrical geometry that is cyclically repeated around the perimeter of the generator. With a cyclic boundary condition this symmetry is utilized to reduce the computational area. This approach reduces the computational effort considerably and enables a straight forward use of moving band in the air gap. The same approach is used here for a linear generator. Although this implies that the influence of the longitudinal ends will be ignored and the field is assumed to be repeated infinitely.

Internal moving boundary is a technique used to facilitate the modeling of motion. This is a method similar to the moving band method [37]. In this method the moving part and the static part are modeled and meshed separately and they are joined by a mutual boundary in the air gap. By cyclically permute the connection point in the mutual boundary, motion can be simulated without re-meshing the geometry. Again the computational gain is significant.

The computational domain and the boundary conditions used here are illustrated in Fig. 2.13.

2.7.3 Magnetic material modeling

The laminated ferromagnetic steel in the stator is modeled by a single valued BH-curve. The BH-curve is obtained through laboratory measurements on stacks with the laminated steel subjected to a altering magnetic field with a frequency of 50 Hz. The influence of the eddy currents at a frequency of 50 Hz are thus included in the BH-curve but the hysteresis is not taken into account.

The steel lamination has a thin insulating layer on each side, which will create a space between the steel in the stator stacks. In order to model these spaces the BH-curve is compensated with a stacking factor:

$$k_s = \frac{d_{steel}}{d_{steel} + d_{coat}}, \tag{2.41}$$

where d_{steel} is the thickness of the steel and d_{coat} is the thickness of the insulation.

The permanent magnets are modeled with the *current sheet approach* [38]. For a uniformly magnetized body the magnetization current, given by (2.25), will be zero in all points inside the body and the magnetic moment are attributed only to *surface current density*, $\mathbf{K}_s$, which are given by:

$$\mathbf{K}_s = \mathbf{M} \times \mathbf{n}, \tag{2.42}$$

where $\mathbf{n}$ is the unit vector normal to the surface. The surface current will flow on all surfaces, which have a component parallel to the magnetization. In the current sheet approach the magnetization of the permanent magnets are modeled by thin current sources at the sides of the magnet which are parallel to the axis of magnetization. This is illustrated for a rectangular permanent magnet in Fig. 2.14. The amplitude of the current is given by integrating (2.42) along the side of the magnet, which for a rectangular magnet is equal to multiplying the thickness of the magnet, h_{mag}, with the magnetization:

$$I_{pm} = h_{mag} \cdot M, \tag{2.43}$$

where the magnetization is set to the remnant magnetization, M_r, of the permanent magnet. The small susceptibility of the magnetization is modeled separately by adding a relative permeability of the magnet equal to the recoil permeability, μ_{rec}.

The losses are calculated in a post process. Eddy current loss, hysteresis loss, and excess loss are calculated from the maximum magnetic field distribution B_{max} and the fundamental frequency ω, which are inserted into (2.34), (2.36), and (2.37), respectively. The material parameters are determined from the experimental BH-curve for the electric steel. This method of modeling iron losses is thoroughly described by Mi *et al.* [39].

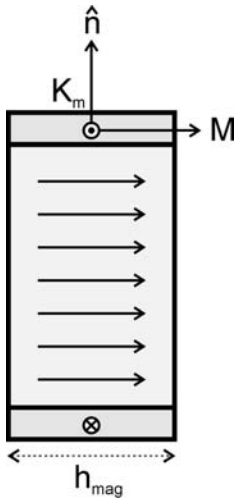

Figure 2.14: Surface current of a rectangular permanent magnet.

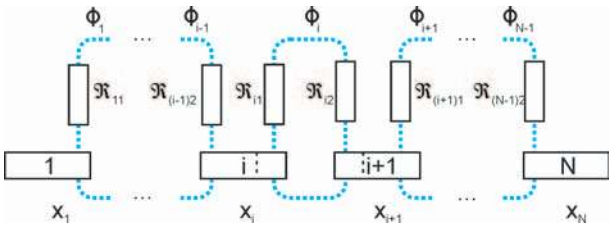

Figure 2.15: Magnetic reluctance model of linear generator including longitudinal end effects.

2.8 Longitudinal end effect model

The magnetic circuit of a linear machine differs in one significant way from rotary machines, since it is open in both ends. The cyclic symmetry of a rotary machine will thus be interrupted in a linear machine by the *longitudinal ends* of the machine. The general mathematical description presented here gives an analytic expression that models the influence of the longitudinal ends.

In order to arrive at a closed analytic form, we only consider the reluctance of the air gap and the permanent magnet. This simplification gives negligible errors in circuits where saturation is low, since the magnetic reluctance of the steel will be much smaller than that of the air gap and the permanent magnets.

An illustration of the model is shown in Fig. 2.15. The model consists of N magnets forming $N-1$ flux paths. The outermost magnets are assumed to be entirely coupled with the inward adjacent magnet, which is equal as setting the reluctance to infinity outside the the generator ends. The flux from the other magnets is divided into two flux paths, one shared with each of the adjacent magnets. The free parameter x_i models, as to what fraction of the flux, is coupled with the right and left flux paths, respectively.

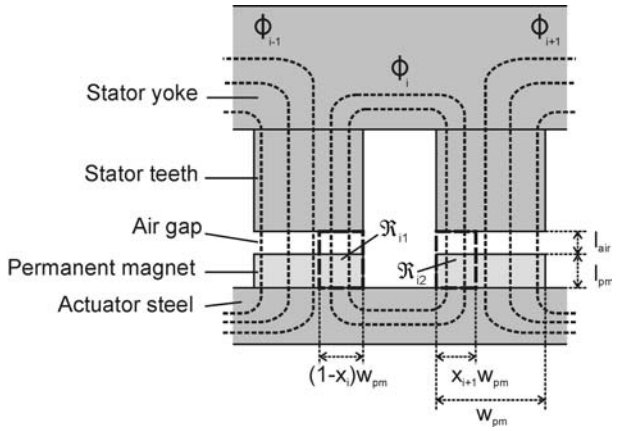

Figure 2.16: Model of magnetic circuit where the flux of every magnet is divided into two flux paths.

The magnetic circuit used in the model is illustrated in Fig. 2.16. The flux path Φ_i will pass two permanent magnets and two reluctances $\Re_{i1}$ and $\Re_{i2}$. The reluctances will depend on the free parameters x_i and x_{i+1} as follows:

$$\Re_{i1} = \frac{\Re_c}{(1-x_i)} \tag{2.44}$$

$$\Re_{i2} = \frac{\Re_c}{x_{i+1}}, \tag{2.45}$$

where $\Re_c$ is a constant, determined by the fixed parameters, such as permeability and geometry. The permanent magnet is modeled with constant magnetization. The amplitude of the magnetomotive force mmf_{pm} will thus be determined by fixed parameters, such as magnet length l_m and remanent magnetization M_r. The flux ϕ_i can be expressed as follows:

$$\phi_i = \frac{2mmf_{pm}}{\Re_{i1}+\Re_{i2}} = \frac{2mmf_{pm}}{\Re_c}\frac{x_{i+1}(1-x_i)}{x_{i+1}+(1-x_i)}. \tag{2.46}$$

The flux in the whole generator will exist in such a way that the magnetic energy is minimized. Magnetic energy density is given by:

$$u_{mag} = \frac{B^2}{2\mu}. \tag{2.47}$$

The magnetic energy associated with one flux path ϕ_i will be the sum of the volume integrals of the magnetic energy density in $\Re_{i1}$ and $\Re_{i2}$. The magnetic induction, in turn, will be given by the amplitude of the flux and the cross-section area of the flux. The expression for the magnetic energy in one flux

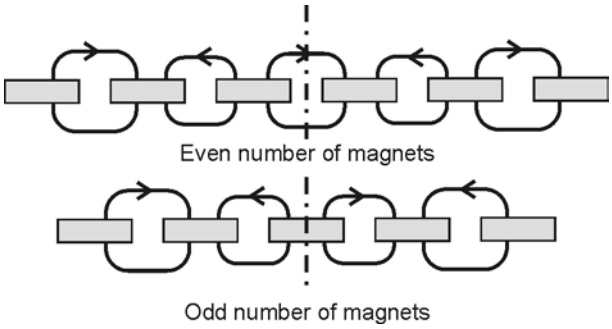

Figure 2.17: Symmetry lines for linear magnetic circuits with even and odd number of magnets.

path is given by:

$$\begin{aligned} U_i &= \frac{1}{2\mu}\int_{\Re_{i1}} \frac{B^2}{2\mu} dV + \frac{1}{2\mu}\int_{\Re_{i2}} \frac{B^2}{2\mu} dV \\ &= \frac{1}{2\mu}\left(\frac{\phi_i}{A_{i1}}\right)^2 A_{i1} l_{stack} + \frac{1}{2\mu}\left(\frac{\phi_i}{A_{i2}}\right)^2 A_{i2} l_{stack} \\ &= \frac{l_{pm}}{2\mu l_{stack} w_{pm}}\left(\frac{\phi_i^2}{(1-x_i)} + \frac{\phi_i^2}{x_{i+1}}\right). \end{aligned} \tag{2.48}$$

Here the the flux is assumed to be homogeneous and the volumes are given by the cross section areas $A_{i1} = (1-x_i) w_{pm} l_{stack}$ and $A_{i2} = x_{i+1} w_{pm} l_{stack}$. The total magnetic energy of the system will be the sum of the energies of the magnetic fluxes:

$$U_{mag} = \sum_{i=1}^{N-1} U_i\left(x_i, x_{i+1}\right). \tag{2.49}$$

To solve the above problem we need to utilize symmetry. A schematic illustration of two linear magnetic circuits with even and odd numbers of magnets, respectively, is shown in Fig. 2.17. Since there is nothing distinguishing the ends of the magnetic circuit except for the sign of the mmf, the *amplitude* of the outmost fluxes ϕ_1 and ϕ_{N-1} will be equal. This holds true also for ϕ_2 and ϕ_{N-2} and so on. For the same reason the free variables will have symmetry of the form:

$$x_i = 1 - x_{N+1-i}. \tag{2.50}$$

If the circuit consists of an even number of magnets, there will be an odd number of flux paths of which $N/2-1$ have a mirror counterpart and a unique flux, $\phi_{N/2}$, in the middle. The sum of the flux paths magnetic energy can then be expressed as:

$$U_{even} = 2\sum_{i=1}^{N/2-1} U_i\left(x_i, x_{i+1}\right) + U_{N/2}\left(x_{N/2}, x_{N/2+1}\right). \tag{2.51}$$

If the circuit consist of an odd number of magnets there will be an even number of flux paths all having an anti-symmetric counterpart on the other side of the symmetry line. The total magnetic energy for an odd number of magnets can then be expressed as:

$$U_{odd} = 2 \sum_{i=1}^{(N-1)/2} U_i \left(x_i, x_{i+1}\right). \tag{2.52}$$

To find the minimum of the total magnetic energy for the even and odd numbered case we set all partial derivatives of (2.51) and (2.52) equal to zero. We get the equation system for the even and odd numbered cases as (2.53) and (2.54), respectively:

$$\frac{\partial U_{even}}{\partial x_i} = \begin{cases} 2\frac{\partial}{\partial x_i} U_i \left(x_i, x_{i+1}\right) + 2\frac{\partial}{\partial x_i} U_{i-1} \left(x_{i-1}, x_i\right) = 0 \\ \\ \text{for } i = 2, 3, ..., N/2 - 1 \\ \\ \frac{\partial}{\partial x_{N/2}} U_{N/2} \left(x_{N/2}, x_{N/2+1}\right) + 2\frac{\partial}{\partial x_{N/2}} U_{N/2-1} \left(x_{N/2-1}, x_{N/2}\right) = 0 \end{cases} \tag{2.53}$$

and for the odd numbered case:

$$\frac{\partial U_{odd}}{\partial x_i} = 2\frac{\partial}{\partial x_i} U_i \left(x_i, x_{i+1}\right) + 2\frac{\partial}{\partial x_i} U_{i-1} \left(x_{i-1}, x_i\right) = 0$$

$$\text{for } i = 2, 3, ..., (N-1)/2. \tag{2.54}$$

All equations are the same form except for the last equation in (2.53). If we insert (2.48) into the general form in (2.53) and (2.54) and only consider solutions with the free parameters in the interval $0 \leq x_i \leq 1$, we get the following recursive equation of second order:

$$x_{i-1} = \frac{1 - x_i - x_i x_{i+1}}{1 - x_i}. \tag{2.55}$$

This number sequence is uniquely determined if the values of two 'independent' variables are known. Since the fluxes of the outermost magnets are assumed to be entirely coupled with the adjacent magnets we know that:

$$x_1 = 0 \tag{2.56}$$

$$x_N = 1. \tag{2.57}$$

However, those two variables are not independent since they both have the same position relative the symmetry line in magnetic circuit and represent the same term in (2.51) and (2.52). We will need a second, independent variable for each system. For the even numbered case we will use the last equation

in (2.53) combined with the symmetry condition (2.50) to get the additional conditions for the recursive equation. When N is an even number we see from (2.50) that:

$$x_{N/2} = 1 - x_{N/2+1}. \tag{2.58}$$

Inserting this into the last equation of (2.53) give us:

$$x_{N/2-1} = 1 - x_{N/2}. \tag{2.59}$$

Inserting this result into (2.55), we can by induction see that the explicit formula for x_i must be on the form: $x_i = 1 - x_{i-1}$. Using the condition (2.56), gives us the explicit formula for the free parameters in a magnetic circuits with even number of magnets:

$$\begin{aligned} x_i &= 0 \qquad i = 1,3,\ldots,N-1 \\ x_i &= 1 \qquad i = 2,4,\ldots,N \end{aligned} \tag{2.60}$$

We will again use symmetry to find the second variable for the recursive equation (2.55) for the odd numbered case. From Fig. 2.17 we see that:

$$x_{(N-1)/2} = 1/2, \tag{2.61}$$

for odd N. We now have two independent variables, which determines the number sequence of the recursive equation (2.55). The derivation of the explicit formula for the odd numbered case is a bit more cumbersome than for the even numbered circuits. Inserting (2.61) into (2.55), and repeating several times with the result, gives a relation on the form $x_i = x_i(x_{i+1}, i)$. From this we can derive the relation between x_i and x_{i+2}. It turns out that this expression is linear in i and we can find an explicit solution by assuming a linear relation between x_i and x_{i+2}. Using the boundary condition (2.56) and (2.61) gives us the explicit formula for the free parameters in a magnetic circuits with odd number of magnets:

$$\begin{aligned} x_i &= \frac{i-1}{N-1} \qquad i = 1,3,\ldots,\leq (N+1)/2 \\ x_i &= 1 - \frac{i}{N+1} \qquad i = 2,4,\ldots,\leq (N+1)/2, \end{aligned} \tag{2.62}$$

where the free variables x_i, for $i > (N+1)/2$, are given by (2.50). The flux distribution in the linear reluctance model in Fig. 2.17 is now fully determined by (2.60), for even numbered circuits, and (2.62) for odd numbered circuits. Knowing the free parameters we can calculate all the fluxes ϕ_i from (2.46). For the even numbered case we will simply have:

$$\begin{aligned} \phi_i &= 0 \qquad i = 1,3,\ldots,N-1 \\ \phi_i &= \frac{mmf}{\Re_c}, \qquad i = 2,4,\ldots,N \end{aligned} \tag{2.63}$$

and for the odd numbered circuit:

$$\begin{aligned} \phi_i &= \frac{mmf}{\Re_c}\frac{N-i}{N} \qquad i = 1,3,\ldots,\leq (N+1)/2 \\ \phi_i &= \frac{mmf}{\Re_c}\frac{i}{N}, \qquad i = 2,4,\ldots,\leq (N+1)/2. \end{aligned} \tag{2.64}$$

The flux from every magnet will be the sum of two adjacent flux paths. For the even numbered circuits the total flux per magnet will be:

$$\phi_{pole,i} = \frac{mmf}{\Re_c}, \tag{2.65}$$

which holds for all magnets. For the odd N we will have two cases, one for even magnets and one for odd:

$$\begin{aligned} \phi_{pole,i} &= \frac{mmf}{\Re_c}\frac{N-1}{N} \qquad i = 1,3,\ldots,\leq (N+1)/2 \\ \phi_{pole,i} &= \frac{mmf}{\Re_c}\frac{N+1}{N} \qquad i = 2,4,\ldots,\leq (N+1)/2. \end{aligned} \tag{2.66}$$

3. Linear generators

In many applications that involves linear (straight) motion it is advantageous to utilize linear machines since the mechanical interface often can be reduced compared with systems based on rotating machines. The application ranges from train propulsion and large conveyor systems to single coil sterling engine generators. There exists today a large number of different linear machines types [40, 41].

In this chapter the linear generators are put in a wave energy context and the machine topology investigated in this work is presented.

3.1 Differences between linear and rotating generators

The internal structure of a linear machine often origins from a rotating machine, where the linear machine is the cut and unrolled version of the rotating machine. A rotating machine and its linear counter part are illustrated in Fig. 3.1. There are however some marked differences in both the functioning and design of linear machine.

The actuator motion of a linear generator is in most cases reciprocal and the speed varies continuously as the actuator accelerates and decelerates near the turning points. This will give a varying frequency of the induced voltage and, furthermore, the order of the phases in a multiphase machine will be interchanged when the actuator changes direction. A direct coupling of a linear generator to a utility grid is thus practically impossible. This problem is addressed in [25] for wave energy applications where also a number of connection solutions are presented.

Although most magnetic circuits of linear machines are based on rotating machines there is one significant difference — a linear machine will have open magnetic circuits in both ends, whereas the magnetic circuit of a rotating machine forms a closed circle. These *longitudinal ends* of a linear machine has influence on the magnetic flux inside the machine and also permits the active area of the air gap to vary as the actuator moves in and out of the stator.

Finally, the supporting structure of a linear generator differs from that of a rotating machine. In contrary to a rotating machine, a linear machine cannot use one axis to fix the actuator but will need several points of fixation to maintain the geometry of the air gap.

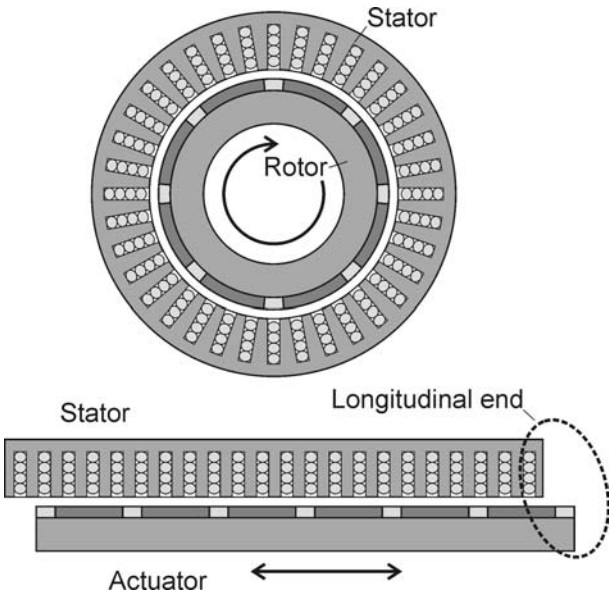

Figure 3.1: Rotating electric machine and its linear counterpart.

3.2 Basic conditions

Using a directly coupled linear generator as power take-off in the wave energy plant reduces the structure and mechanic components to a minimum, but poses new requirements on the generator. Those requirements are to a great extent determined by the nature of the ocean waves. The two most obvious differences to conventional generators are the slow speed and the large variation in power.

The slow speed is a direct consequence of the direct drive concept. The speed of the actuator will, to a first approximation, be determined by the vertical speed of the sea surface, which is in the order of 1 m/s. This is 30 – 50 times slower than conventional synchronous rotational generators and the reaction force, consequently, needs to be 30 – 50 times larger to give the same out put power. To achieve that high reaction force a direct drive generator will need to be larger than a high speed generator.

The generated power will vary both on a short timescale, due to the varying actuator speed, and on a longer time scale, due to the changing wave conditions. In paper IX the behavior of the plant is investigated at different wave conditions with a first order force model[1]. Figure 8 in the paper show the output power for small, medium and large waves and it can be seen that power both on a short term, as well as on longer term, varies considerably. The absorption factor is however reduced as the power in the waves increases. Four mechanisms are identified that explains the reduction in absorbed power

[1] Only the displaced water volume is considered in the force calculations. Hydrodynamic forces are neglected.

Table 3.1: *Basic conditions for the design study.*

Parameter	Value
Nominal speed	0.7 m/s
Nominal power	10 kW
Reaction force at nominal power	14.3 kN
Long term overload	2 – 5 times nominal load
Short term overload	$\geq$10 times nominal load
Pitch length	> 1.5 m
Load	Passive rectifier

namely, the damping of the generator, the buoy height, the spring constants, and the pitch length. This is explained further in the paper.

The *long term overload* will be determined by the most extreme wave condition at the site and the absorption factor of the plant. Even though the absorption factor is expected to be reduced as the wave power increases, the maximum long term overload could be expected to be several times higher than the annual average power of the generator.

Since there is no intermediate power storage in the wave energy converter the output power will be determined by the instantaneous speed of the actuator. The maximum *short term overload* resulting from steep wave front impinging on the device is a difficult task to estimate. However, sudden peaks reaching 10 times larger power than average power is not impossible to be encountered.

Even though the power of the generator varies continuously, it is useful to define a nominal power. We will define the nominal power as the power produced when the actuator is moving at the average vertical speed of the sea surface of a *nominal wave*. The nominal wave used throughout the work is a sinusoidal wave with a height of 1.6 meters and a period of 4.6 seconds, which gives an average vertical speed of 0.7 m/s. The nominal wave is chosen rather freely based on a wave climate from the Baltic Sea [42]. The nominal power is set to 10 kW, and the generator should thus produce 10 kW at an actuator speed of 0.7 m/s. The nominal output power is adapted for a point absorber of 3 – 4 m width and a relatively moderate wave climate. In more energetic climates the power rating should be larger.

The stroke length of the generator should be matched to the wave heights and is the range of meters. Compared with other linear machine application this is a relatively long pitch length. Furthermore, a passive rectifier will be employed and the load current and load voltage will thus be in phase. The basic conditions for the generator is summarized in Table 3.1. It is stressed that the overload estimations are preliminary guesses.

3.3 Linear generators for wave energy conversion

A number of different linear machines have been proposed for wave energy applications. Induction machines can on an early stage be ruled out since they cannot compete with the permanent magnetized machines at the slow speed at hand [43]. An analysis of different machine types suitable for marine renewable energy conversion is presented in [44].

A lot of focus have been put on the machine types known as *transverse flux permanent magnet machines* (TFPM) or *variable reluctance permanent magnet machines* (VRPM)[2]. The TFPM was introduced by Weh *et al.* [45] and has been investigated for wave energy applications by Mueller *et al.* [21], and more generally, by Harris *et al.* [46]. Both the TFPM and VRPM are capable of producing very high force-to-weight ratio, thus they can be made relatively small for a given output power. The geometry of TFPM and VRPM machines permits a very high armature flux and can possibly have a very high force per pole. The drawback with these types of machine is the relatively small permanent magnet flux per pole and a high synchronous inductance, which will give a load angle in the range of 57°–70° [47]. Phase compensation [48] or some kind of power converter with high power rating [21] is needed to fully appreciate the generator performance. Another drawback is the relatively complex stator composition, which is made of several independent C-cores of laminated steel.

Lately, an air cored tubular permanent magnet generator has been suggested for wave energy applications [49]. By removing the steel in the stator the normal forces are virtually eliminated. This is a large constructional advantage, however, the machine needs to be considerably larger to compensate for the low magnetic flux in the coil windings.

In this thesis a linear permanent magnet synchronous generator with longitudinal flux is studied. This generator type has an inherently small load angle and the stator construction is simple and robust. A similar generator has been investigated with analytical methods [22] and employed in the off-shore testing of Archimedes Wave Swing wave energy converter.

3.4 Longitudinal Flux PM Generator

A cross-section of the magnetic circuit of the generator is illustrated in Fig. 3.2. The main magnetic flux, created by the permanent magnets, is illustrated with dashed lines and the direction of the flux is indicated with arrows. The magnetic flux from one magnet traverses the air gap and is conducted by the stator teeth through the stator coils. In the stator yoke the flux is divided into two paths, which return through the stator teeth, via the air gap and through the adjacent magnets. The steel plate in the actuator connects the magnetic

[2]The classification is somewhat vague and both types could be considered as being one class

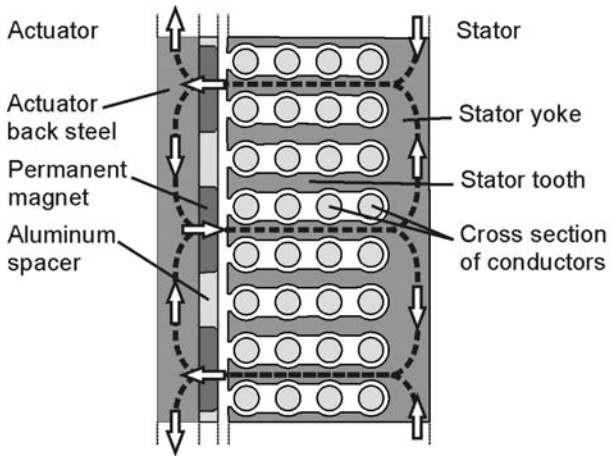

Figure 3.2: Cross-section of magnetic circuit of a permanent magnet synchronous generator. The actuator is to the left and the stator is to the right.

flux at the back of the magnets. The magnetic circuit consists to a large extent of ferromagnetic steel, which serves to reduce the magnetic reluctance of the circuit and to guide the flux past all stator coil windings.

3.4.1 Cable winding

A three phase winding is employed, which means that three sets of coils are used, internally shifted $2/3$ pole width. A three phase system is able to deliver constant power flow, whereas a single phase system unavoidably will have a power varying with the double frequency of the current.

In order to reduce the cogging we use a fractional winding configuration. Cogging is a force that is due to the non homogeneous stator reluctance, *i.e.* the magnets tend to cling to the stator teeth. In a non-fractional winding the actuator and the stator will have a symmetry that is repeated every pole width and the cogging force of every magnet will add to the others resulting in strong fluctuation of the forces. In a fractional winding this symmetry is broken and the cogging force is reduced considerably [50]. Here we use a fractional winding with a *number of slots per pole and phase* of $q = 6/5$. The winding configuration is illustrated in Fig. 3.3.

The phase windings are made of standard cables with circular cross-section. The copper conductor is made of individual strands and is very flexible. Easy handling and low price are the main motives for choosing this cable. In the manufacturing process some 1000 meters of cable need to be wound into every generator and the winding procedure will represent a substantial part of the manufacturing costs. The 1 mm thick PVC insulation gives a short time dielectric strength of 20 kV, can withstand 70° C in continuous operation, and has long lifetime both in air and in sea water.

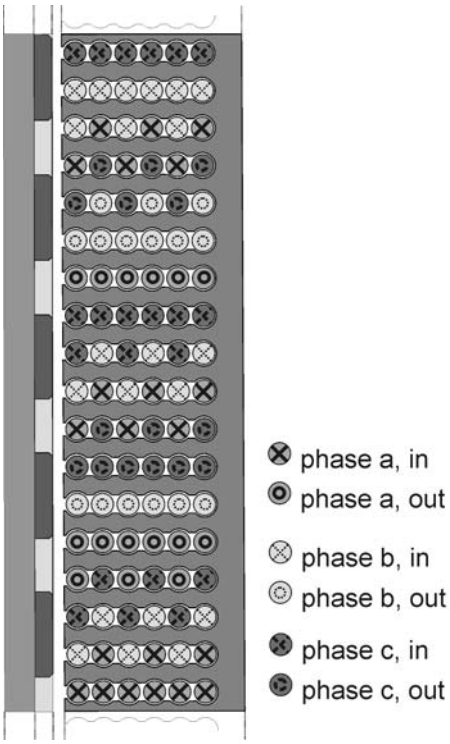

Figure 3.3: Cross section of a segment of the generator illustrating the fractional winding configuration.

3.4.2 Permanent magnets

The magnetic material used is the rare earth magnet Neodymium–Iron–Boron (Nd–Fe–B), which has the highest energy product of all materials known today. A comparison between Ferrite magnets and Nd–Fe–B magnets show that the generator can be up to 10 times smaller with Nd–Fe–B magnetized main flux [51].

The properties of the Nd–Fe–B are summarized in Table 3.2. The Nd–Fe–B magnets are sintered and manufactured with high precision. The magnets are very brittle and highly corrosive, hence are coated with a thin layer of nickel to protect from corrosion.

3.4.3 Stator steel

The stator is made of laminated electric steel with a thickness of 1 mm. Most electric steels are adapted for a frequencies of 50 Hz or higher and this is one of the thickest commercially available electric steel. When the number of plates are limited, *i.e.* for a prototype, the steel sheets are cut individually with laser. In serial production the sheets are cut with a punching tool. The magnetic properties are somewhat deteriorated near the cuttings both after

Table 3.2: *Material properties of Nd–Fe–B permanent magnets.*

Parameter	Value
Remanent magnetic induction B_r	1.277 T
Recoil permeability μ_{rec}	1.02
Intrinsic coercive field H_{ic}	1.08 kA/m
Temperature dependence H_{ic}	0.1 %/K
Temperature dependence B_r	0.7 %/K

laser cutting and after punching. This has larger influence where the geometry is narrow, *e.g.* the stator tooth.

4. Design

The design study takes its starting point at the basic conditions, set by the waves and the converter concept. The electromagnetic behavior of the generator is modeled with finite element method, which takes into account the varying actuator motion and the outer circuit. Several hundred simulations have been carried out where different parameters and working conditions have been studied.

One of the goal is to optimize the design of the generator. Optimizing, however, means choosing and a choice that seems optimal one day will in the light of new knowledge and varying basic conditions be sub-optimal the other. An equally important goal is therefore to build a knowledge foundation that can be the base for future optimization studies.

This chapter is based on the work presented in the two papers I and II. A more extensive discussions regarding the prerequisites for this generator and the design can be found in the papers.

4.1 Finite element based design

An in-house developed software is utilized throughout this thesis[1]. The numerical method is described in chapter 2.7. Both steady state simulations, where the actuator speed is constant, and transient simulations, where the actuator speed is continuously varying, is utilized in the design process. The geometry and the results are be visualized in graphs and some examples of the visual output from the software are given in Fig. 4.1. A number of important parameters, such as absolute loss components, load angle, total material weight, etc., are also obtained.

Finite element modeling provide a very accurate and detailed modeling of the electromagnetic behavior of the generator. By making incremental changes of one parameter, it possible to study that parameter's influence on the machine performance. But, one needs to keep in mind that the parameters are not independent and that the results always have to be interpreted in the light of basic knowledge of electric machine.

Finite element based simulations is the foundation of the design study. Over five hundred simulations form the basis of the first prototype generator presented in chapter 5.2.

[1] Developed by Dr. A. Wolfbrandt and Dr. K.E. Karlsson

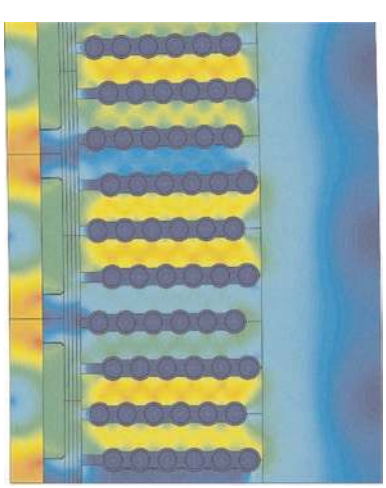

(a) Magnetic density distribution

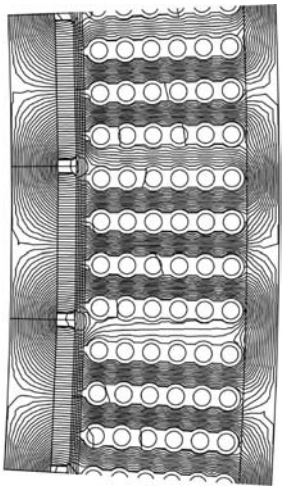

(b) Magnetic flux lines

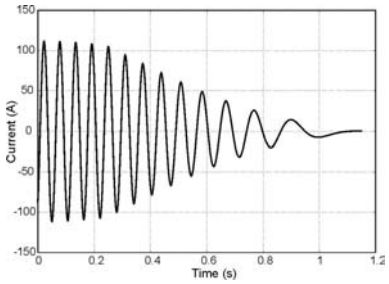

(c) Currents

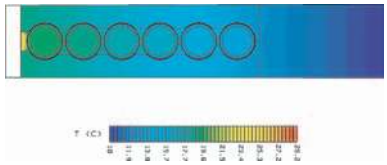

(d) Temperature distribution

Figure 4.1: Output from finite element software

4.2 General design considerations

To develop the needed reaction force the generator have to be considerably larger than a conventional high speed generator with the same power rating. In contrast to a conventional generator, where the design to a larger extent is determined by the thermal loading, the heat generation is a minor problem for this generator since the generated power per volume is so small. The main issues in this generator are the *size*, the *efficiency*, and the *load angle*. The goal of the design study is to construct a small generator with high efficiency. In contrast to other wave energy converters where the generator only is a minor component, this generator will actually carry a large part of the total construction cost of the wave energy converter. A reduction in generator size will directly reflect the cost of the total plant. Furthermore, the efficiency has a direct influence on the energy delivered to the grid and will thus affect the annual revenue of the plant.

There is no obvious reason to optimize with respect to the load angle, since it is already taken into account in the simulations. However, the load angle

at nominal load determines how much more the output power, and thus the damping of the generator, can be increased. Some sea conditions may imply that the generator is heavily damped. A small load angle at nominal load allows large changes in generator output power. Furthermore, the load angle will increase if the actuator speed is increasing. Low load angle at nominal speed vouch for preserved performance at higher speed.

4.3 Load current

As a direct consequence to the large size, the stator winding will be longer and the cable resistance relatively higher, compared with a conventional generator. The resistive losses is the dominating losses in this generator and the current level needs to be relatively low in order to maintain high efficiency. The influence of the current level is investigated in paper II, where the efficiency, size, and load angle for different current/voltage levels are given, see Fig. 6, in the paper.

The efficiency of the machine will increase with lower current due to the reduction of resistive losses and the load angle will decrease, accordingly with (2.9). In the meantime, the size of the generator needs to be larger in order to achieve the higher voltages, see (2.12). There will obviously be a trade-off between performance and size in this case.

4.4 Magnetic circuit

By designing an efficient magnetic circuit we can increase the force per air gap area without changing the load current. In this case both the machine size and the losses is decreased.

The force in the air gap is a result of the interaction between the two major magnetic field in the generator — the permanent magnet induced flux and the stator winding induced armature flux. According to (2.19), the force in a generator with resistive load is proportional to the product of the amplitudes of the permanent magnet flux and the armature flux multiplied with the cosine of the load angle.

The load angle for a machine with resistive load is given by (2.9). By comparing the equations (2.15), (2.18), and (2.10) we see that the quota in (2.9) is proportional to the quota between the armature flux and the main flux, giving rise to the relationship $I_{ph}\omega L_s/E \propto B_a/B_{pm}$. The quota between the armature flux component and the permanent magnet flux component is thus a figure of merit, which determines the load angle of a generator with resistive load. To keep the load angle limited it is clear that, in a machine with resistive load, B_{pm} should be the dominating term. This is cleverly described in [47].

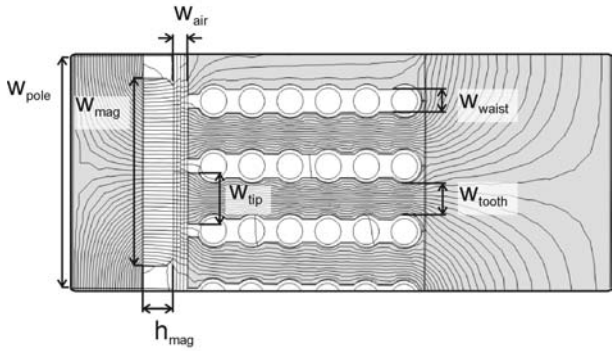

Figure 4.2: Cross section of one pole with the magnetic flux lines at load.

The load angle can also be reduced by minimizing the armature winding leakage flux, see (2.15). By minimizing leakage flux we can decrease the load angle, without affecting the armature winding flux.

Different flux components in the magnetic circuit can, to a large extent, be controlled by the design of the magnetic circuit. The influence of pole width and number of cables per slot is investigated in the paper II. Permanent magnet design and stator steel geometry is thoroughly analyzed in paper I. These papers demonstrate that the design of the magnetic circuit in many aspects is a trade-off between different properties. The cross section of one pole with the magnetic flux lines at load is illustrated in Fig. 4.2. The flux lines illustrates the resulting flux of both the permanent magnet flux and the armature flux.

4.4.1 Numbers of cables per slot

By increasing the number of conductor in every slot we can decrease the number of poles with preserved total number of coil turns. The number of poles and thus the size of the generator can thus be reduced with maintained no-load voltage, see (2.11). The total number of coil turns will remain more or less the same, but since the main inductance of a circuit is proportional to the square of the number of turns in each coil, see (2.14), we will see an increase in the synchronous inductance. The influence of number of cables per slot are investigated in paper II. Efficiency, generator size, and load angle for different number of cables per slot are given in Fig. 7 in the paper. The size goes down steadily for increasing number of cables companioned with a growing load angle. The efficiency is increasing marginally for larger number of cables due to the reduced iron losses. An extra effect revealed by the finite element simulations is an additional increase in the load angle. This is due to an increase in the leakage flux caused by the longer stator teeth.

The results can also be interpreted in terms of flux components. Increasing the number of turns per slot increases the proportion of armature flux wave in

the air gap and, in accordance with the discussion above, we will have a larger load angle.

The largest number of cables are limited to 10. Higher number of cable would require a different design where the cables are lying in two rows to limit the length of the stator teeth. This is an interesting alternative not yet further investigated.

4.4.2 Pole width

The pole width determines the frequency of the permanent magnet flux, which will be increasing with smaller pole widths. The pole width also sets the limit for the width of the stator teeth, w_{tooth}, illustrated in Fig. 4.2. The stator teeth form a bottleneck in the magnetic circuit and the teeth width determines to a great extent the total flux in the magnetic circuit. If the flux is assumed to be proportional to the pole width, as in (2.11), the induced voltage will be independent of the pole width. However, due to the slots, an increase in the pole width will give a larger increase in the flux than the corresponding decrease in the frequency. Consequently, the induction per pole will increase for larger pole widths.

In paper II, different pole widths are simulated and the resulting performance is illustrated in Fig. 8, in the paper. Generator size will increase for larger pole widths. This is in accordance with the discussion above. We will also see improved performance for larger pole widths. Even though the machine length is larger, the total number of poles is reduced. This will give a shorter cable length, which explains the amelioration in efficiency.

4.4.3 Permanent magnet design

Although the price of Neodymium Iron Boron magnets have lowered the last years, the material will stay relatively expensive, since it contains the rare earth metal boron. An efficient use of the magnet is thus promoted for economical reasons. Two aspects are investigated in paper I, namely the size and the shape of the magnets. The size of the permanent magnet has influence on both efficiency, total size of the generator, and the load angle. The efficiency, stator length, magnet volume, and load angle for different magnet sizes are illustrated in Fig. 3 in the paper. All parameters are ameliorating with increasing magnet size, however at the cost of increased total magnet volume. This can be understood by considering that an increase in the permanent magnet size means an increase in the main flux component. This, in turn, increases the force per pole and reduces the load angle. The machine size can thus be reduced and, as a consequence, the losses will be lower. Again, we have a trade off between performance and cost.

The amelioration stagnates, however, at a point where an increase in magnet size only gives a smaller reduction in load angle. The efficiency and size

remains, on the other hand, constant. This is due to the saturation of the steel in the stator teeth. An increase in magnetomotive force in the magnetic circuit is counteracted by an rapidly growing reluctance. Larger magnet height, h_{mag}, also reduces the magnetic coupling between the actuator and stator.

The influence of magnet shape is illustrated in Fig. 4 in the paper where the magnet height, h_{mag}, and magnet width, w_{mag}, is altered with the total volume fixed. The result demonstrate, that for this specific setup, the magnet should be as flat as possible. It can by analytical means be showed that for smaller magnets the optimal relation between height and width is almost equal to the ratio of the air gap width, w_{air}, and the width of the magnet. This shape would for the investigated magnet size yield magnets wider than the pole width, w_{pole}, which explains that the optimum is observed for the widest magnet.

4.4.4 Stator steel geometry

The main purpose of the stator steel is to guide the magnetic flux through the entire coils. This means maximizing the main flux and minimize leakage fluxes. The stator steel can be cut with large freedom and the geometry can be tailored with high accuracy to achieve desirable properties. Some of the design choices are obvious, as they give both improved main inductance and reduced leakage flux. In many cases, however, a change in geometry will give an increase in both the main inductance and the leakage fluxes. Here, there will be a trade-off between size and load angle.

The influence of different tooth tip width, w_{tip}, and waist, w_{waist}, is analyzed in paper I. A larger tooth width at the air gap increases the effective air gap area and the flux coupling between the actuator and stator will thus be larger. On the other hand, a too wide, w_{tip}, provides a mean for the magnetic flux to take a short cut and leakage flux will thus increase. An illustration of the influence of different, w_{tip}, on the flux pattern is given in Fig. 9 in the paper. The result show that the tooth tip has minor effect on the machine size, but a large tip will give a considerably larger load angle. Similar results are obtained for different widths of the waist, w_{wais}, where smaller waist gives small reduction in size but a large increase in load angle. The flux lines and the iron losses for different, w_{waist}, are given in Fig. 7 and 8 in the paper.

4.5 Design of test generator

Based on the study presented, a design was decided for a first test generator. The main features of the design is presented in Table I in paper II. This generator design is optimized with regard to high efficiency and low load angle, rather than machine size.

A thorough analysis of the performance of this generator design is undertaken in in section 5 in the paper II. The performance at nominal load and

Table 4.1: *Main characteristics of test generator*

Parameter	Value
Nominal power	10 kW
Main voltage	200 V (r.m.s.)
Total air gap area	2.08 m^2
Load angle	6.6°
Efficiency	86.0 %
Hysteresis losses	0.53 kW
Eddy current losses	0.04 kW
Resistive losses	1.0 kW

constant air gap area is summarized in Table II, in the paper. The most important characteristics are also given here, in Table 4.1. The efficiency is rather high for this kind of generator. As can be seen the losses are dominated by the resistive losses, which represent 64% of the total electromagnetic losses. Hysteresis losses contributes to 33%, whereas eddy current losses are almost negligiable. This is a consequence of the low frequency. Hysteresis losses are proportional to the frequency (2.36) and the loss density will be low. However, due to the large size the total loss will be important. Eddy current losses, on the other hand, are proportional to the square of the frequency, see (2.34), and will consequently be very low.

The phase voltages, when the actuator is moving at sinusoidal speed, are illustrated in Fig. 10 in the paper. When the actuator is 0.25 m off center, it starts to slip out of the stator and the active air gap area will become smaller. As a consequence to this, the induced no-load voltage will go down at the turning points. This is reflected as an additional decrease in the voltages, which is visible in the figure.

Two overload cases are also investigated, one with 100% overload and one with 300% overload. The speed of the actuator is increased, but the load resistance is the same as for the nominal load case. Simulations of the heat distribution in the generator at overload is illustrated in Fig. 11, paper II. The simulations suggests that the temperature in the generator will be moderate even at 300% overload. However, thermal simulations are very much determined by the boundary condition. Heat transfer coefficient between stator and the surrounding structure is only estmated and the result is a rough estimation of the thermal behaviour of the machine.

5. Experimental generator

Many of the problems associated with a realization of a new machine cannot be anticipated beforehand, and some of the difficulties that you have worried about, may prove to be of less importance in the real case. The best way to identify true problems and avoid focusing on "constructed" problems is to build and test the machine.

The test generator was constructed to resemble, as far as possible, the generator that would be employed in the wave energy converter concept. Apart from the engineering aspects, an experimental set up is also important to verify the numerical model.

5.1 Construction

The experimental generator is illustrated in Fig. 5.1. The magnetic circuit of the generator is the one presented in the previous chapter, however, the length of the actuator and stator is somewhat shorter. The length of the stator was set to 700 mm and the actuator is 650 mm, both having a width of 400 mm giving an active air gap area of 1.04 m^2. We will thus have a generator with shorter actuator than stator. The generator has four sides with the square shaped actuator in the middle and four separate stator packages on the outside facing the actuator sides.

The piston can move vertically and is fixed with eight bearings, which run along rails mounted on a center pillar. The center pillar is connected with the stator packages at the top and the bottom through a steel framework structure. This supporting structure is necessary to maintain a constant air gap width and to counteract the significant attractive forces that is developed between the actuator sides and the stator packages. Springs are mounted on the side and connected to the bottom of the actuator by ropes running through blocks. This is not the preferred solution in a real wave energy generator, where the springs should be attached directly to the actuator.

The upward motion of the actuator is provided by a hoist system, which in the first test is connected to an over head crane, and later on to an asynchronous motor. Gravity and the springs provide the force for the downward motion.

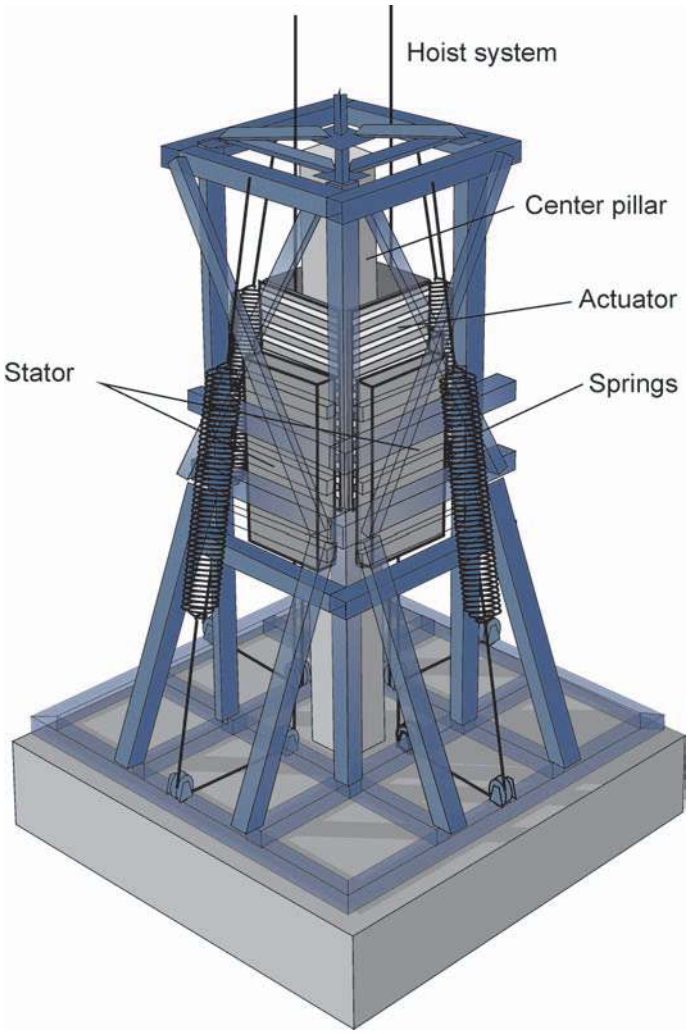

Figure 5.1: Illustration of experimental generator. The support structure is made transparent over the active parts of the generator.

5.1.1 Stator cable winding

The stator cable windings can be threaded freely, as long as the phase and direction of the cable follows the winding pattern illustrated in Fig. 3.3. There is thus a large number of possible end winding configuration. The winding pattern used was optimized to give minimized total end-winding length and to give an even distribution of the end-windings. The principles of the winding is illustrated in Fig. 5.2, which shows the path of one phase. The packages where wound separately and connected in series.

Due to the design of the stator slots, see Fig. 4.2, the cable has to be threaded from the side of the stator packages. Every threading adds wear to the cable insulation. To limit the number times that a cable needs to be threaded through

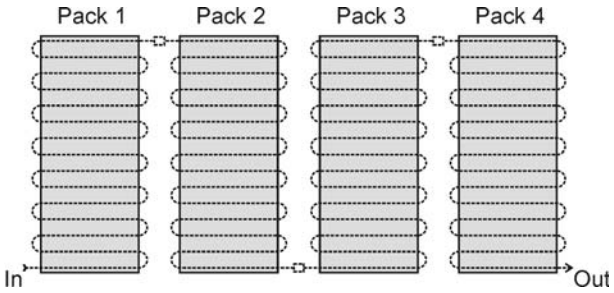

Figure 5.2: Schematic illustration of the winding path of one phase. Every stator packages is wound separately and connected in series when mounted on the support structure.

the stator, every phase was divided into six cables and the winding of every cable is started in the middle of each stator package. The number of times that the same part of a cable needed to be thread was in this manner reduced to 8 – 10 times.

5.1.2 Normal air gap forces

The actuator and stator will be attracted to each other by magnetic forces. By using a multiple side actuator, these forces can be reduced, since the forces of the opposing sides of the actuator act in different directions. However, the forces increases rapidly with decreasing air gap widths and a small horizontal displacement of the actuator will give a resulting force on the actuator, acting in the direction of the smallest air gap.

The dynamics of the normal forces on a multiple sided linear generator is investigated in paper VI. With finite element method modeling, using Maxwell's stress tensor method [52], the dynamic normal forces in the generator was calculated at no load for different air gap widths. In Fig. 7 in the paper, the normal force, is given for an air gap of 3.0 mm, for a moving actuator. The force varies, as the actuator moves, due to a similar mechanisms that causes cogging. The maximum force is 11.3 kN per pole and meter of stacking length, which would give a resulting force for one side of the experimental generator of 58.8 kN. The maximum normal force, for air gaps widths ranging from 1 to 6 mm, are given in Fig. 8 in the paper. It can be noted that the force increases rapidly for smaller air gap widths. The resulting force for different actuator displacement from an original 3 mm air gap is illustrated in Fig. 10 in the paper. A displacement of 1 mm, from an origin 3 mm air gap, would for this experimental generator yield a force of 29.6 kN working to increase the displacement.

The actuator is thus in an unstable equilibrium where a small displacement will give a force working to increase the displacement. In order to avoid total collapse of the air gap, the supporting structure needs to be stiff enough to

provide a restoring force that is growing more rapidly with the displacement than the magnetic force.

The stator packages where fixed to the supporting structure with adjustable bolts and, once the actuator was in place, the stator packages where adjusted successively from a very large air gap toward smaller air gap widths. The smallest realizable air gap width was 5 mm, which is 2 mm larger than the original design.

5.2 Experiments

The numerical method is used extensively in the design of the generator and it is important to verify the accuracy of the tool for future design studies. A thorough investigation of the numerical tool is carried out in paper III where simulated results are compared with experimental results from the prototype generator.

5.2.1 Magnetic field distribution

Magnetic induction is measured in the in the air gap with a Hall-effect flux probe. In Fig. 3, paper III, the normal component of the magnetic induction in the air gap, measured along a vertical line, is compared with simulated values. These measurements revealed that there is noticeably lower flux for the first and third magnet in the measurements, whereas the numerical model predicts a symmetric air gap flux distribution. This is attributed to the longitudinal ends, which are ignored in the numerical code, see section 2.7.2.

A comparison of simulated and measured magnetic induction along a horizontal line is shown in Fig. 4 in the paper. The measurements are carried out in front of the third magnet row from the top, and are thus systematically lower than the simulated values. The influence of the permanent magnet joints and the the edges of the air gap are also clearly visible in the graph. However, the flux around permanent magnet joints and fringing flux at the air gap edges give negligible impact on the total flux, as depicted in the paper.

5.2.2 Slow speed

A first set of measurements where conducted with the existing over head crane and presented in paper II. The speed was then limited to 67.5 mm/s, which is approximately 1/10 of the nominal speed. A Y-connected, purely resistive load with 4.0 Ω resistance were connected and the voltage were measured over the resistances. The air gap width was set to 5 mm. The results are illustrated in Fig. 13 in the paper, where the measured phase voltages are plotted together with the simulated voltages at the same actuator speed.

The simulated and the measured voltages correspond well. The linearly varying envelope, reflects the change of active air gap area, as the actuator slides in and out of the stator. There are, however, some discrepancies, mainly in the shape of the voltages and in the relation between the phase amplitudes. This can partly be attributed to the varying speed of the actuator due to cogging forces, which in turn influences the shape of the voltage curves. Moreover, longitudinal ends introduce a disturbance in the magnetic flux pattern that is non-symmetric with respect to the different phase windings. This could explain why the experimental phase voltages do not have the same internal relation as the simulated ones. Longitudinal end effects are treated in Chapter 7.

5.2.3 Nominal speed

A hoist system with a 75 kW induction motor[1] was connected to the test generator [53]. A speed up to 0.86 m/s is possible to achieve, but the air gap has now been increased to 7 mm. The voltage of one phase, measured over a Y–connected resistive load of 5 Ω, is presented together with simulated values in Fig. 5 in paper III.

Again, the experimental and simulated values show good agreement. The experimental values are now smother than in the low-speed experiments. This is probably a result of smother actuator speed, due to larger damping, and lower cogging forces, due to larger air gap width.

5.3 Air gap width measurement sensor

A sensor was developed[2], which is able to measure the air gap width during operation. The sensor design and experimental results are presented in paper VII. The sensor is of a search coil type and the operation is passive, *i.e.* no power feeding is needed. It consists of a coil etched on both sides of a printed circuit board, that measures $30.3 \times 8.1 \times 0.36$ mm. The sensor is illustrated in Fig. 5.3 The sensor is placed on a stator tooth in the air gap and will generate a voltage signal that is proportional to the time derivative of the coupled magnetic flux, in accordance with Faraday's law of induction, see (2.2). The sensor signal for different air gap widths is illustrated in Fig. 8 in the paper. The air gap width is continuously changing as the actuator moves, which is reflected in the sensor signal. Integrating this signal with respect to time will give a signal proportional to the magnetic flux.

The air gap flux is determined by a number of factors, of which the air gap width and the stator currents are the two most important. To determine the air

[1] Master thesis by M. Stålberg

[2] Master thesis by R. Waters

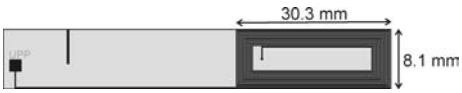

Figure 5.3: Search coil sensor.

gap width during operation, we need to find the mapping between the sensor signal and the air gap width, for different load currents.

A method was developed, where the definite integral between two zero crossings of the sensor signal is mapped with the corresponding air gap width. This was conducted for air gaps widths ranging from 4.0 to 9.5 mm at no-load. The result from several runs is illustrated in Fig. 11 in the paper, where a second degree polynomial fitting is used to find the mapping function. According to these result the air gap width can be determined from the sensor signal with ± 0.4 mm accuracy to a certainty of 95%. The accuracy of the method is believed to be improved significantly, if the measurements of the air gap width is improved. The measurments are today conducted by hand with a slide caliper and not at the same time as the collection of the sensor signal.

To fully appreciate the sensor, a mapping matrix is needed where different sensor signals and load currents can be mapped with a specific air gap width. This mapping matrix could be established through a combination of experiments and simulations, where experiments would give accurate results and means to calibrate the simulations and simulations would be used for working conditions difficult to simulate in a laboratory.

6. Full scale offshore experiments

The most important step when developing a new technology is to test it during real conditions. Full-scale on-site testing of the wave energy converter adds a number of new challenges, but will also give information and experiences impossible to be obtained in a laboratory. For the first time, we will be able to see the full dynamics of the wave energy plant and we will be able to study factors such as power absorption, long and short term overload, survivability, length of life, power quality, etc. But maybe most important is to evaluate the numerous technical solutions employed in the wave energy converter.

The first wave energy converter was launched and connected to land on March the 13th 2006. This wave energy converter is the first of a total of 10 complete wave energy converter commissioned for the Lysekil Wave Energy Project[1]. In parallel to the technical research, a biological study is being performed, which investigates the impact of the plant on the environment [54]. The construction of the plant was mainly carried out by S. Gustafsson, U. Ring, E. Strömstedt, M. Stålberg, O. Svensson, and R. Waters.

6.1 The wave power plant

The plant is illustrated in Fig. 6.1. The generator is placed inside a watertight steel structure, which is mounted on a concrete foundation. The linear motion is translated by a piston through a water tight piston sealing. The rope is guided at the top of the structure by four rolls, which ensure that the the piston forces only has a vertical component. The buoy is cylindrical and has a diameter of 3 m and a height of 0.8 m and is connected to the piston with a Vectran rope. The plant is placed at a depth of 25 m and the structure is pressurized continuously during the submersion to a final pressure of 2.5 bar. A sub-sea cable connects the test site with a land station. The cable is 2.9 km long and is dimensioned to deliver power from 10 converters. The on-shore measurement station is equipped with heat sink resistive loads, that are mounted on the outside of the house.

[1] http://www.el.angstrom.uu.se/

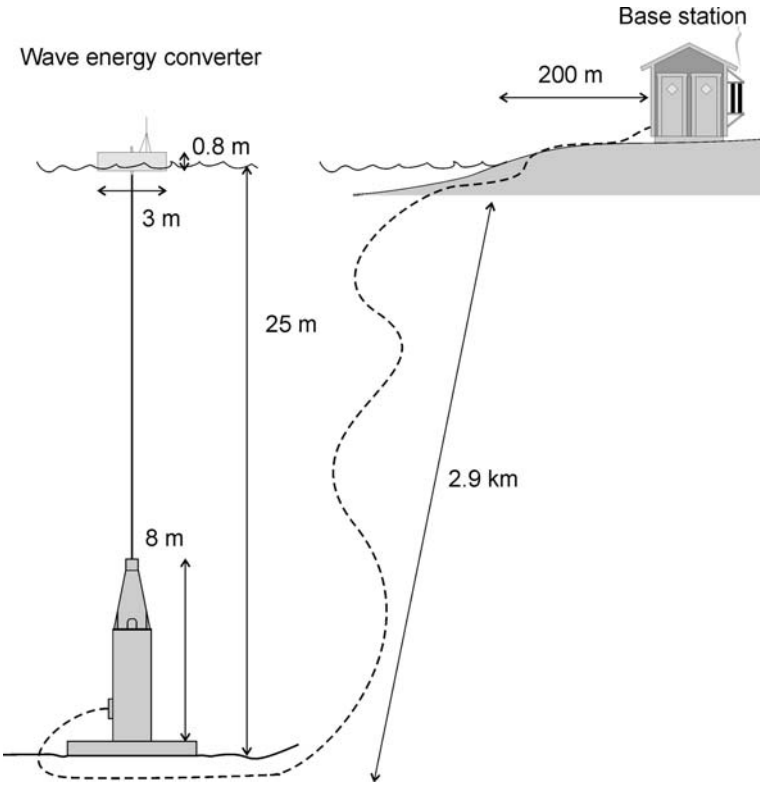

Figure 6.1: Schematic illustration of the wave energy converter.

6.1.1 Generator

The magnetic circuit has the same design as the laboratory generator except for some small modifications. The waist, w_{waist}, is now slightly decreased and sharp corners in the slots are rounded in order to minimize ware on the cable in the winding process. The length of the stator was increased to 1265 mm, the length of the actuator to 1865 mm, and the stacking length is 400 mm. The total air gap area is thus increased to 2.0 m^2. The actuator is now 600 mm longer than the stator, giving a pitch length with constant air gap area equal to 600 mm. The total pitch length is 1800 mm.

An illustration of the generator can be found in Fig. 6.2. The support structure differs significantly from the laboratory prototype. The bearings of the actuator are now traveling on hardened steel rails mounted *directly* on the stator structure. This results in a considerably stiffer structure and an air gap width of 3 mm was achieved without problems. Eliminating the center pillar also gives space for the 9 springs, which now are mounted inside the actuator and attached between the top of the actuator and the bottom of the steel structure.

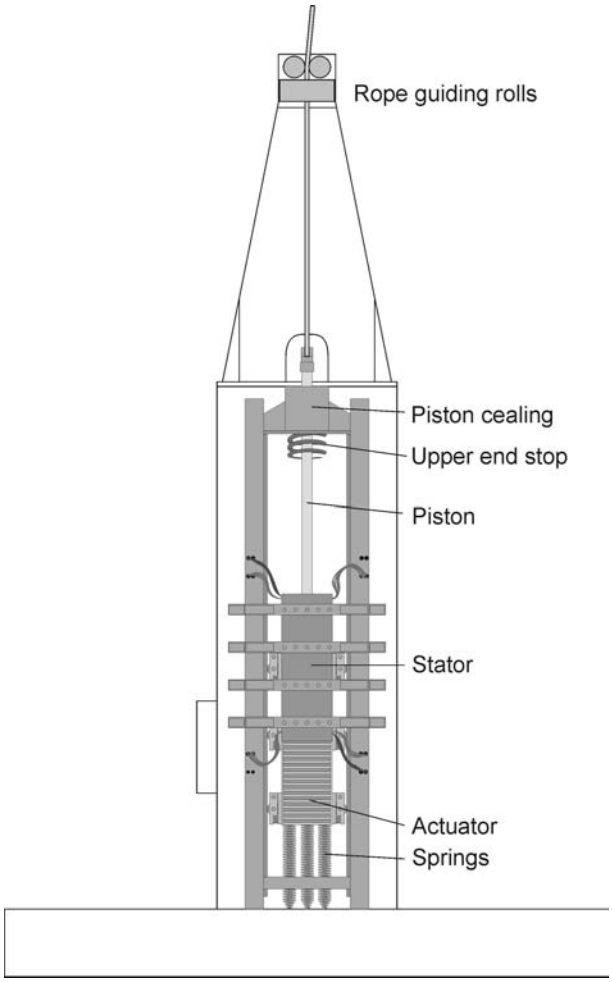

Figure 6.2: The offshore generator inside the watertight steel structure.

6.1.2 Electric system

At this stage the phase voltages are not rectified in the plant. One reason for this is to reduce the risk of failures but, from an experimental point of view, it is advantageous to have the phase voltages delivered to the base station where all the measurements are being performed.

The electric system is illustrated in Fig. 6.3. The phases of the generator are Y–coupled to three of the conductors of the sub-sea cable and the fourth conductor is utilized as a common ground. The phases are Δ–coupled to a purely resistive load. The load resistances can be varied in the range 1.5 – 20 Ω. A resistance R_{earth} of 1 kΩ is placed between the generator and the ground.

A lumped circuit of one phase is illustrated in Fig. 6.4. This model only holds for symmetric voltages. Small errors can be expected since the system has non-symmetric voltage components. The generator is represented by the

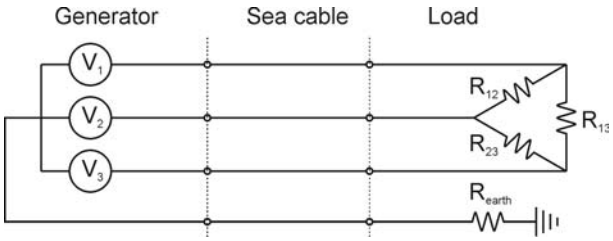

Figure 6.3: The electric circuit of the off shore plant.

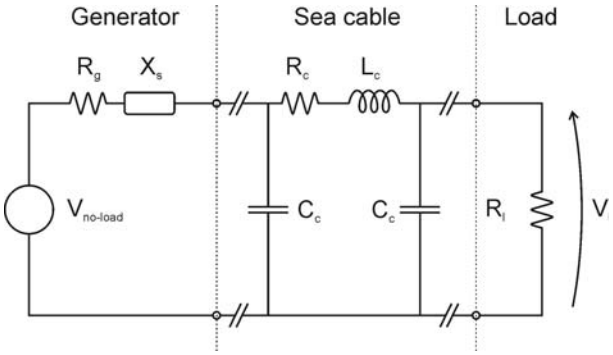

Figure 6.4: Lumped circuit diagram of one phase.

no-load voltage, the winding resistance and the synchronous inductance, as described in section 2.2.1. The cable is modeled by a π-circuit, where the total capacitance of the cable is divided into two equal capacitances placed on each side of the cable resistance R_c and the cable inductance L_c.

The values of the components in the lumped circuit are listed in Table 6.1. The capacitances are dominating over the inductances in the sub-sea cable and it will thus act as a phase compensating element to the inductive component that origins from the generator inductance. The resulting load voltage will thus be slightly larger than for a system where cable capacitance is ignored. However, the influence of cable capacitance is small and the load voltage and will increase only by 0.3 %.

6.2 Measurements

The load voltages are continuously measured by computer based system and stored. High frequency recordings have been collected manually by oscilloscopes. From the main voltages we can directly calculate the power in the load voltages. By using the lumped circuit model, illustrated in Fig. 6.4, we can estimate all important electrical entities in the system, such as resistive losses in generator and cable, no-load voltage, load angle, etc. The total electromagnetic power can thus be calculated, if we include the iron losses given

Table 6.1: *Component values of one phase lumped circuit of the wave energy converter.*

Component	Lable	Value
Cable winding resistance	R_g	0.45 Ω
Synchronous inductance	L_s	12.5 mH
Sub-sea cable resistance	R_c	0.54 Ω
Sub-sea cable inductance	L_c	ignored
Sub-sea cable capacitance	C_c	145 μF
Load resistance	R_l	0.51 – 6.7 Ω

by the numerical model, see Table 4.1. Moreover, both the position and speed of the actuator can be determined from the phase voltages, knowing that two successive zero-crossings of one phase corresponds to a movement of the actuator by one pole width[2].

In parallel to the voltage measurements, a wave measuring buoy is recording the waves approximately 50 m from the wave energy converter [55]. Although the waves hitting the wave energy converter are not identical to the waves that the buoy measures, statistical parameters such as significant wave height and zero crossing period will be the same.

Some of the first results from the are treated in paper IV. The phase voltages, the relative position, speed of the actuator, and the power in the load, for a time sample of 100 seconds is illustrated in Fig. 2 in the paper.

The voltages are varying in both amplitude and frequency. A typical pattern is formed as the waves cause the buoy to rise and fall. The inlets in the top figure show a zoom on the resulting voltage from a wave crest, where the first peak is generated when the actuator is pulled upwards by the buoy and the second as it is pulled downward by its own weight and the springs. A significant difference in the envelope of the voltages can be noticed. The first voltage peak has an almost sinusoidal envelope, which is a result of a sinusoidal actuator speed. The second peak, on the other hand, has an envelope that is decreasing linearly after the maximum is reached. This phenomenon have also been predicted in paper IX for larger waves and it is concluded that this occurs when the downward speed of the buoy exceeds the maximal speed at which the springs and gravity can pull the actuator.

The lower graph show the power production, which is varying considerably. The peak powers are, during this time sample, about six time higher than the average power.

[2]The load voltage has a phase shift with regard to the no-load voltage determined by the electric system and the frequency of the voltage. Neglecting the phase shift gives small errors in the estimation of the position (in the range of 2–4 mm), but will render noticeable error on the speed estimation if the phase shift is changing rapidly due to fast change in the actuator speed. Compensating for changing phase shift is, however, gruesome since it in practice involves a twofold time differentiating of the original signal, with significant distortion as a consequence.

6.3 Power absorption for different damping factors

One important factor of the hydrodynamic behavior of the plant is the damping factor of the generator. Power absorption of the plant varies considerably with different damping factors [56]. The damping factor is given as the force developed for a certain speed:

$$k_{damp} = \frac{F}{v}. \tag{6.1}$$

This can be rewritten in terms of power by using the relation $P = F \cdot v$ where we get:

$$k_{damp} = \frac{P}{v^2}. \tag{6.2}$$

The power of the plant will be proportional to square of the induced emf, see (2.7), which, in turn is proportional to the speed. Hence the load factor will, if non-linear effects are ignored, be independent of the speed. Furthermore, by changing the load resistances, the damping factor of the plant can be varied.

In paper IV, the behavior of the plant at different sea conditions and at different loadings is investigated. The load resistance has continuously been varied over a period of 2.5 months. In Fig. 3 in the paper, the absorbed average total power of the system is compared with the prevailing wave power densities, which is calculated from the data provided from the wave measuring buoy. Three different loadings are investigated — 2.2Ω, 4.9Ω, and 10.0Ω. The lower load resistances are not realistic for this generator since they will result in a very poor efficiency. Nevertheless, it is interesting to study the wave energy converter behavior for a wide range of damping factors. The result indicates an optimal damping factor for the plant with respect to power absorption, in the tested interval.

7. Longitudinal ends

The longitudinal ends adds an element of asymmetry to the magnetic circuit not encountered in the rotating generators. This asymmetry is often neglected and the magnetic flux distribution is often assumed to be symmetric, both in analytical [57, 58, 59] and numerical models [60] of linear machines.

However, during the course of this work the influence of the longitudinal ends has been manifested several times. Measurements of the magnetic induction in the air gap revealed that longitudinal ends, not only affect the flux of the outermost magnets, but also creates an asymmetry, which is spread inwards in the machine (see section 5.2.1). Other artifacts, such as large cogging forces, induced the suspicion that longitudinal ends plays a larger role in the machine behavior than earlier suspected.

In this chapter the longitudinal end effects are described and the mechanisms governing the longitudinal ends influence on the magnetic flux distribution is investigated with both an analytic method and by FE-method. A derivation the analytical model and the main features of the longitudinal end effects can be found in paper V.

7.1 Static longitudinal end effect

In a rotating generator, the flux from one magnet follows the stator teeth and is divided into two, more or less equal, flux paths in the stator yoke, which follows the stator teeth back and form closed paths through the adjacent magnets. The magnets can be said to be *equally coupled* with their neighboring magnets. Such a distribution is advantageous since the flux in the stator yoke and rotor will be evenly distributed and saturation in these parts is reduced. The flux lines from a section of a rotating machine is illustrated in Fig. 7.1.

However, in a linear generator the outermost magnets will only have one return path in the stator steel and will thus couple most of its flux with the adjacent magnet inside the generator. The two outermost magnets will then be *pairwise coupled*. The third magnet will find the second magnet occupied with the first and will thus couple most of its flux with the fourth magnet. The disturbance, caused by the longitudinal ends, is in this manner transferred inwards in the machine. The flux lines in a linear machine are illustrated in Fig. 7.2.

There are however mechanisms that counteract this pair wise coupling, one being symmetry and the other is saturation. If the magnetic circuit has an odd

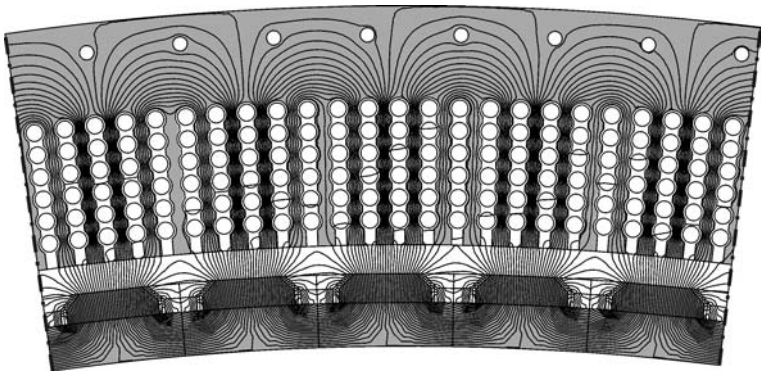

Figure 7.1: Magnetic flux lines in a section of a rotating generator. The pattern is repeated cyclically around the whole generator perimeter

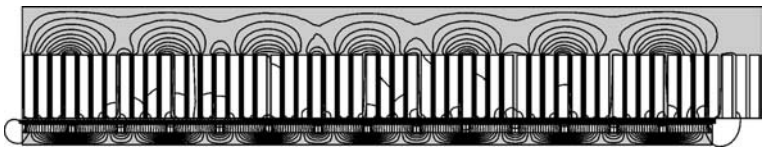

Figure 7.2: Magnetic flux lines in a linear generator.

number of magnets, the flux of the middle magnet will, due to symmetry, be divided equally between the neighboring magnets. The flux distribution will thus be governed by two opposing demands and the resulting flux will be a pattern which converts, from a coupled flux pattern at the ends, toward an evenly distributed pattern in the middle. In a circuit with even number of magnets there are no middle magnet and there will be no symmetrical constrains on the pairwise coupling. The symmetry mechanisms is studied with a linear analytical method in the next section.

Saturation will punish the uneven flux distribution in the stator yoke and actuator back steel caused by the pairwise flux coupling. The pair wise coupling will thus will be counteracted by saturation and again an equilibrium between two opposing forces will result in a coupled flux pattern near the ends that transforms into an more even distribution near the middle. The influence of saturation is studied in section 7.3 by comparing linear and non-linear FE-modeling of the full geometry.

The literature on static longitudinal end effect is sparse. Additional harmonics in the induced voltage and torque due to static longitudinal end effects have been shown with classic reluctance modeling [61]. The *dynamical longitudinal end effect*, on the other hand have become the object of a number of studies, principally concerning linear *induction* machines [62, 63]. This effect is also caused by the asymmetry introduced by the longitudinal end, but in contrary to the static longitudinal end effect, it depends on the speed of the actuator and is consequently small at lower speeds. Dynamic end effects have

also been studied for synchronous machines both experimentally [64] and numerically with space harmonic analysis [65]. End effects have been studied with three dimensional FE-methods for air cored linear generators and a reduction in torque have been noticed [66]. The influences of the longitudinal ends are however very different in an air cored generator and cannot be compared with longitudinal end effect encountered when the stator is made of steel.

7.2 Analytic reluctance model

An analytic model, described in section 2.8, has been developed in order to quantitatively describe the flux distribution in a linear machine. A shorter version of the derivation is given in paper V. The model is based on a linear reluctance model, where the flux of every magnet is distinguished into two paths, see Fig. 2 and 3 in paper V. Since only linear parts are taken into account saturation effects will be neglected. The result is a general closed expression, which gives the flux in the right and left path for every magnet. The model shows that there is a fundamental difference between linear circuits with odd and even number of magnets. Hence, different solutions are obtained for even numbered circuits (2.63) and for odd numbered circuits (2.64).

Two examples are given in Fig. 4 in paper V. The upper figure shows the flux distribution for a circuit with odd number of magnets and the lower for even number of magnets. In the even numbered circuit the coupled pattern stretches the whole machine length, whereas, in the odd numbered circuit it is converted into an equally coupled pattern in the middle magnet.

If we study the total flux from every magnet, given by (2.65) for even numbered circuits and (2.66) for odd numbered circuits, we will see again that the two cases have different solutions. In the even numbered circuit, the flux of all magnets will be equal, which is the same behavior as we see in rotating machines. In odd numbered circuit, on the other hand, the flux will be somewhat smaller for odd magnets and higher for the even magnets magnet. This artifact is larger for circuits with a small number of magnets and decreases as the number of magnets gets larger. Uneven air gap flux, is a consequence of Maxwell's third equation, which states that the total flux traversing a close surface is zero. In a two dimensional case, ignoring leakage flux, the sum of all flux crossing the air gap is zero. Since we have a surplus of one polarity, obviously it means that the flux contribution from every magnet cannot be equal.

7.3 Finite element simulations

Linear and non-linear finite element simulations of the full geometry are illustrated in Fig. 6 in the paper. In the linear simulations, the permeability of the iron parts are assumed to be constant. Except for some stray flux, the linear simulations show the same pattern as the analytical model, both for even and odd numbered circuits. The non-linear simulations, on the other hand, show a new phenomena not present in the analytic model, nor in the linear FE simulations. Now the coupled pattern at the edges is transformed and becomes more evenly distributed near the middle even for the even numbered circuit. This is due to saturation mechanism described above, which tends to smoothen out uneven flux distribution.

The saturation mechanism is also manifested in the air gap flux distribution. In Fig. 7, paper V, the vertical component of the air gap flux is given for the the two machines, for linear (top) and non-linear (bottom) simulations. Again, the linear simulations give approximately the same result as the analytic model for both cases. The results from the non-linear simulations diverges from the linear models both for odd and even numbered circuits. In the odd numbered circuit, we see that the uneven air gap flux distribution is accentuated at the edges and somewhat smaller at the center. The even numbered circuit shows the same pattern as the odd numbered circuit — a heavily distorted air gap distribution near the edge, which is transformed into an even distribution in the middle.

The uneven air gap flux arises when the pair wise coupled flux transforms into an equally coupled flux. When this happens, there will be a surplus of half a magnet for one of the polarities involved in the transformation. By the same arguments used for the symmetry mechanism, we can conclude that the different polarities cannot have the same flux. Furthermore, the faster the flux is transformed, the larger the distortion in air gap flux. The result depicted in the lower graph in Fig. 7, reveals that the symmetry and the saturation cooperates. The saturation effect is largest at the edges. The symmetry mechanism, on the other hand, gives the same influence all along the machine length.

7.4 Consequences

The longitudinal end gives rise to a distortion in the flux distribution which in turn will give rise to secondary effects. One of the most alarming effects will occur if the actuator is allowed to leave the stator. When the actuator moves out or into the stator the outermost magnets will also move out or into the stator and the pairwise coupled magnets inside the stator will be forced to change their partners. When this happens, the flux densities in the actuator back iron will change. This is illustrated in Fig. 7.3 for a machine with pairwise coupled flux pattern. The dark circles mark the areas where the flux densities are high

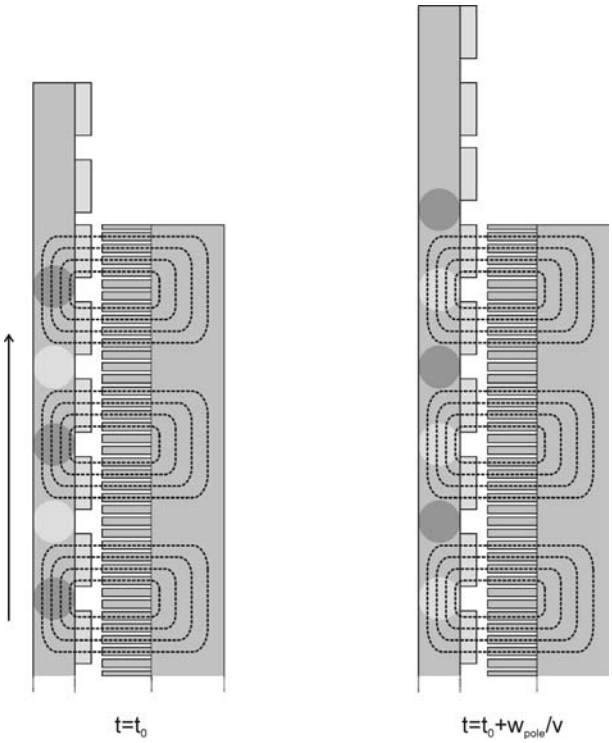

Figure 7.3: Magnetic flux density variation in actuator due to longitudinal end effect as actuator is moving out of the stator

at $t = t_0$ and the light circles where it is low. At $t = t_0 + w_{pole}/v$ the relation is the inverse.

If the actuator of a linear generator is made of solid steel, there could be considerable eddy currents as the fluxes changes. The dimensions of the steel will be much larger than the skin depth, see (2.35). The eddy currents will, consequently, be inductance limited and give rise to considerable reaction fields. In order to fully see the influence of the longitudinal end effects, we will have to study the dynamic and 3-dimensional eddy currents in the actuator.

Another consequence of the coupled flux pattern is that the stator yoke and actuator steel will experience higher flux densities in some parts than in an equivalent circuit without longitudinal ends. This could change the design criteria for these parts.

And finally, the uneven air gap flux distribution interrupts the symmetry that is utilized in fractional pole winding to reduce the cogging forces. The utility of this method is thus decreased.

8. Discussion

8.1 Design

With FE-methods, it is possible to study how small changes in the geometry influences the fluxes in the machine. Figure 8.1, show the flux distribution in the stator teeth for two different tooth tip widths, with the relative changes in air gap flux and load angle given beside the flux distribution. The tooth tip width, together with other parameters, such as magnet shape and slot waist width, are investigated in paper I. By systematic analysis of details in the magnetic circuit, it is possible to maximize the main flux component and reduce the leakage flux. Hence, ameliorate the over all performance of the generator.

However, in most cases there is a trade off between size (cost) and performance. The Fig. 8.2 show the impact of number of cables per pole, with regard to generator size, efficiency, and load angle. The same results are seen for the pole width, the armature current level, and the magnet volume — the performance increases to the cost of larger generator size (paper I and II).

In the trade-off between size and efficiency, economy is the most important parameter. An increase in efficiency will directly be reflected in the energy production of the plant. The cost of the losses can be estimated in the same way as the value of energy production and will depend on factors, such as, lifetime of the plant, electricity price, and interest rate [16]. To get a complete economical model, knowledge of how the generator size relates to the con-

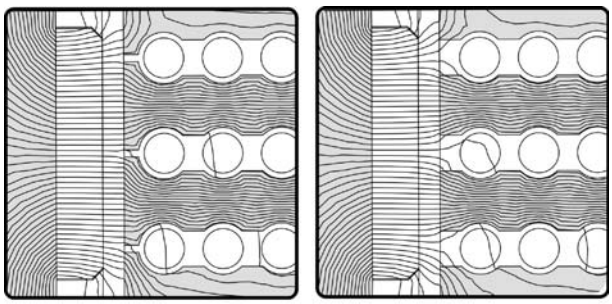

Figure 8.1: The magnetic flux in the stator teeth for two different tooth tip widths.

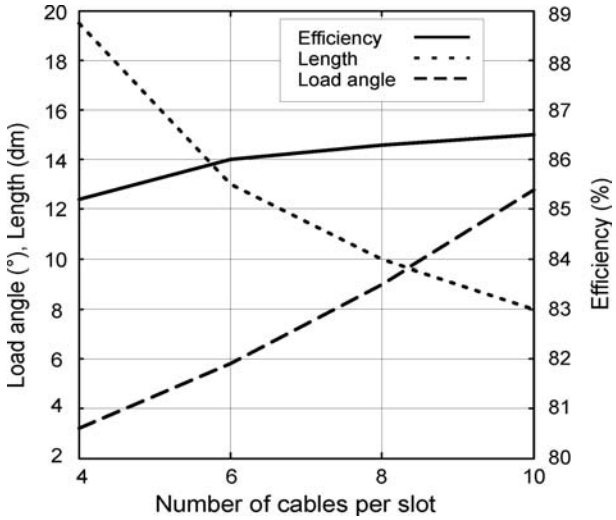

Figure 8.2: Efficiency, generator length, and load angle as a function of cables per slot.

struction costs of the whole plant, is necessary. Furthermore, a good model of how efficiency is related to the size, which was one of the goals of the design study, is needed.

In harsh weather, the generator has to be damped more heavily. The load angle, at nominal load, is a measure of how much the power, and thus the damping factor, can be increased. Result from offshore testings will be vital to be able to estimate the need for over-damping capacity.

8.2 Experiments

The experimental results verify, to a large extent, the numerical tool used in the design process (paper III). However, measurements of the magnetic induction in the air gap revealed that the longitudinal end have larger influence on the magnetic flux distribution than what was expected. The measured and simulated normal component of the magnetic induction in the air gap is illustrated in Fig. 8.3. This discovery led to a thorough investigation of the longitudinal end effects (paper V).

Experiences from the construction of the laboratory prototype show the importance of building a generator, that as far as possible, resembles the generator that would be used in the wave power plant. Many of the lessons learned from the generator prototype, are related to the construction. For example, the air gap forces showed to be of highest importance, whereas the handling of permanent magnet proofed to be much more simple than what was expected. The smallest realizable air gap was 5 mm for the prototype generator. Smaller air gap resulted in complete deviation of the actuator.

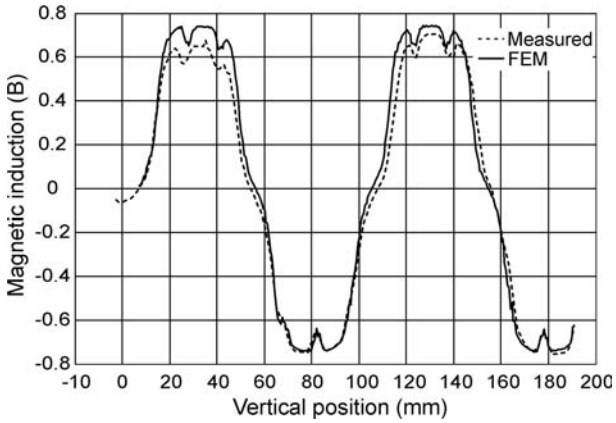

Figure 8.3: The normal component of measured and simulated magnetic induction, along a vertical line in the air gap.

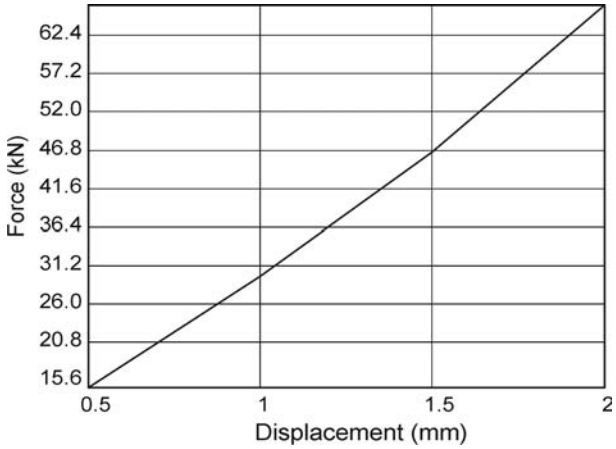

Figure 8.4: The resulting normal force on the actuator, as a function of displacement from an original air gap width of 3 mm.

The unstable equilibrium of the actuator was investigated with FE-simulations (paper VI). The normal forces on the actuator increases rapidly if the actuator is displaced from the center position. Figure 8.4, gives the total normal force on the actuator as a function of displacement. The original air gap is in this case set to 3 mm. A small air gap decreases the reluctance in the magnetic circuit and will thus increases the main inductance of the machine, see (2.14). The electrical performance of the machine can thus be increased but to the cost of larger normal forces in the air gap.

A sensor system, developed in order to be able to monitor the air gap width during operation, was tested on the prototype generator (paper VII). The accuracy of the sensor was estimated to ± 0.4 mm. A number of means to increase the accuracy of the sensor was identified and, in the future, an accuracy of ± 0.1 mm, is probably achievable. Measurements of the air gap width during

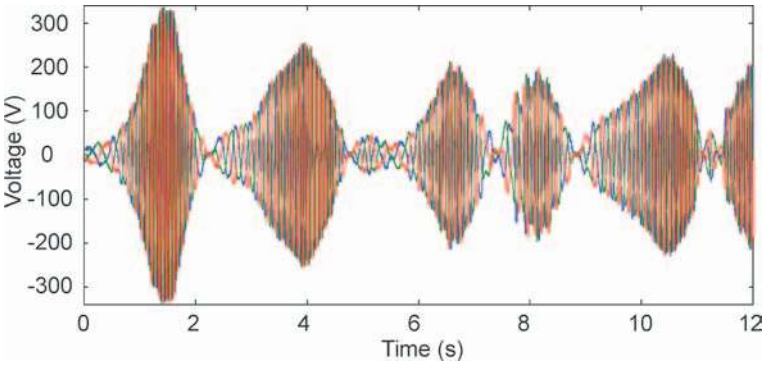

Figure 8.5: Measured main voltages from the Lysekil wave energy converter.

operation would give the data necessary to evaluate, *e.g.*. wear of the bearing system, and also provide an indication of the need for maintenance.

8.3 Offshore experiments

The results from the offshore wave energy converter are based on recordings of the three load voltages in the measurement station on land. From the load voltages, the power in the load can be calculated, and the total power in the system, including losses in generator and sub-sea cable, can be estimated. Furthermore, the load voltages can be used to determine the actuator speed and position. A sample of the main voltages is illustrated in Fig. 8.5. The voltages varies both in frequency and in amplitude as the actuator follows the motion of the waves. As a result, the power will vary over a wave period and the average power is typically six times lower than the peak power. This illustrates the benefit of connecting a large number of units into a plant, and thus to reduce the fluctuation in total power.

The power absorption of the plant have been studied with different load resistances/damping factors (paper IV). The absorbed average power was compared with wave data from a wave measuring buoy. The results show that the absorption of the plant can be governed by changing load resistance. Furthermore, there exists an optimal load resistance for this configuration, in the interval 2.2Ω — 10.0Ω. By changing the load, it is possible to maximize the power at wave conditions with lower power, and more important, the energy absorption can be limited in higher wave conditions. This is an important result, which show that, by means of regulating load resistance (or DC-level), the behavior of the plant can be controlled from shore.

The generator has, during the first test period, been exposed short term overloads, up to 8 times the nominal load, and main voltages of 480 V. These conditions occurred during exceptional events, nevertheless, it proves the robustness of the generator.

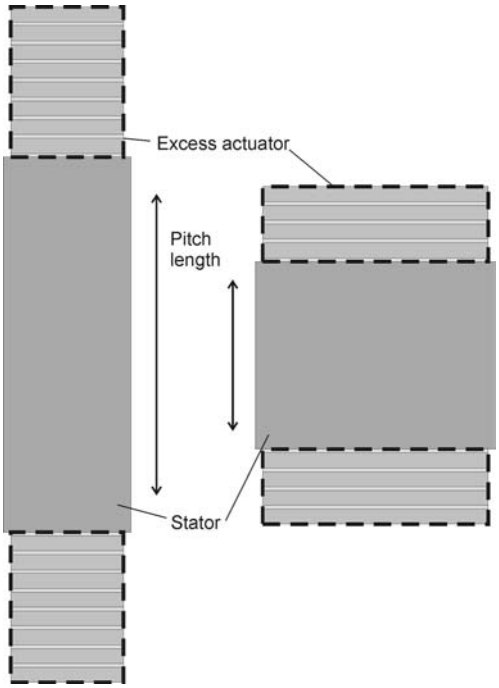

Figure 8.6: Maximum pitch length with constant air gap area for a thin and wide generator width equal total size.

The varying air gap area's influence on the power absorption of the plant is not fully understood yet. However, it is suspected that the changing air gap area reduces the total power absorption. If the actuator is made sufficiently long the air gap area can be constant for the full pitch length. Again, there is a trade off between cost and performance. However, a long and thin generator can have a longer pitch length with constant air gap area compared with a short and wide generator with the same amount of excess actuator area. This is illustrated in Fig. 8.6, which shows two generators with the same area on actuator and stator. There are also drawbacks with longer generators. A longer generator will give a longer total height of the converter. This have implication on the mechanical load on the structure and a larger foundation will be needed. Another drawback is that there will be more end windings which will give a larger leakage inductance.

8.4 Longitudinal end effect

The longitudinal ends' influence on the magnetic flux was revealed in the measurements of the air gap flux on the prototype generator. The longitudinal ends give rise to a distortion in the flux distribution, which spreads inwards in the machine. With an analytical model, it is shown that this is due to a pair wise

coupling of the edge-magnets (paper V). Furthermore, the flux distribution differs between linear generators with even or odd number of magnets in the circuit. By comparing linear and non-linear FE-simulation, the influence of saturation could be studied. It was concluded that saturation counteracts to the pair wise coupling of the flux.

One consequence of the longitudinal end effect is the uneven air gap distribution. This could explain the relatively large cogging forces that was experienced, both with the laboratory prototype and the offshore generator. Another consequence, is that the field strength in the stator yoke and piston back steel, in some areas, will be larger than what the simulations model predicted. These part could, as a consequence, be underdimensioned.

However, most alarming is the dynamic influence of the longitudinal ends. When the actuator is moving out of the stator, the topmost magnet will leave the magnetic circuit, and consequently, the second magnet will have to change its 'coupled partner'. This is illustrated in Fig. 7.3. This will result in a changing flux pattern in the actuator back steel, which in turn will induce eddy currents. This effect is, probably, accentuated if the actuator is longer than the stator.

The load voltage measurement of the laboratory prototype coincide very well with the simulated values, and the longitudinal end effect seems to have small impact on the induced emf. The offshore generator differs from the laboratory prototype in one significant way — the actuator is longer than the stator. Analysis of the offshore data indicate that the induced emf is lower than what was anticipated from the simulations. The reason for this is not yet completely understood, but longitudinal end effects could be the cause.

In order to understand the influence of eddy currents, a dynamical model is needed. Furthermore, the eddy currents will form in the z-direction, and a 3-dimensional model will be necessary. A deeper understanding of the longitudinal end effects is vital, and could possibly induce radical changes in the design of linear permanent magnet generators.

9. Conclusion

This thesis accounts for the development of a new type of generator, from design, via laboratory testing, to a full scale offshore wave energy converter.

A linear synchronous permanent magnet generator has been designed for use in a wave energy converter plant. The design is based on simulations performed with a FE-based simulation tool. The application impose several demands on the generator. For example, the actuator speed is slow, in the order of 1 m/s. As a consequence, the generator needs to be larger than a conventional fast rotating generator. Furthermore, the generator should also be able to endure long term overloads, up to 5 times nominal load, and short term overload, possibly up to 10 times nominal load. Finally, the generator should be adapted for passive rectification, *i.e* the power factor will be equal to one.

By detailed tailoring of the magnetic circuit and deliberate choice of a low current at nominal load, a generator with very low load angle (6.6°) and relatively high efficiency (86%), has been achieved. As a consequence the generator is relatively large. To achieve the rated power of 10 kW at 0.7 m/s, the generator needs an air gap area of 2.08 m^2. The losses are dominated by resistive losses (64%), followed by hysteresis losses (33%), the eddy current losses are almost negligible.

A laboratory prototype was constructed based on the results from the design study. Measurements of load voltage, at a constant actuator speed of 0.067 m/s and 0.86 m/s, corresponds well with the simulations. However, a difference between measured and simulated air gap flux was discovered. This was attributed to longitudinal end effects, which are ignored in the numerical model. However, longitudinal end effect seems to have little influence on the induced emf for this specific set up.

The unstable equilibrium of the actuator, due to strong normal magnetic forces, became apparent during the experimental work. Finite element simulations of the normal forces on a multi-sided permanent magnet actuator show that the forces increase rapidly with the actuator displacement. This, together with the experiences from the laboratory prototype, led to a complete refurbishment of the supporting structure for the offshore generator.

A full scale offshore wave energy converter was constructed and launched outside Lyskil, on the west coast of Sweden. The test proves the viability of the concept and provided vital data of the dynamic behavior of the generator. The power varies continuously, due to the varying actuator speed, and average power is typically six times lower than the peak power. The generator has

endured short term peak powers of up to 8 times the nominal load and voltages of over two times the design voltage.

The load resistance's influence on power absorption was investigated for for a wide range of wave conditions. It was concluded that the load resistance affects the power absorption significantly and there is an optimal load resistance in the interval 2.2Ω – 10.0Ω. This result show how the power absorption of the plant can be controlled from land.

The longitudinal ends' influence on the magnetic flux distribution became apparent during the laboratory experiments. The phenomenon has been described by means of an analytical method and by FE-simulations. Longitudinal end effect give rise to nonsymmetric air gap distribution and flux concentrations in the stator yoke and in the actuator back steel. These effects are believed to have small influence on the over all performance of the generator. A more alarming effect occur when the actuator leaves the stator and the flux pattern in the actuator is forced to change. The resulting effect is not yet clarified and it is stressed that the dynamic influence of longitudinal end effects needs further investigation.

10. Summary of papers

The order of the papers are not strictly chronological. The first four papers follow the outline of this thesis and describe the development work of the linear generator from design, via experiments, to the final offshore experiments. Paper V to VII give more specific accounts of different features of the linear generator. Paper VII to X describes the concept and the research project more generally. The first eight papers are all journal papers and the last two are conference proceedings.

Paper I: Detailed Study of the Magnetic Circuit in a Longitudinal Flux Permanent-Magnet Synchronous Linear Generator

This and the second paper form the basis of the design study that later on led to the first laboratory prototype. Some of the results from the extensive design process, with a focus on the magnetic circuit, are presented here. The advantages of finite element modeling is evident in this paper when the magnetic circuit is fine-tuned on millimeter scale. Most work in this paper was carried out by the author.

Published September 2005 in *IEEE Transaction on Magnetics*,.

Paper II: Study of a longitudinal flux permanent magnet linear generator for wave energy converters

This paper gives a more general account of the generator and puts it in a wave energy context. The design study presented in this paper completes the design process of the laboratory prototype. Simulated results of the chosen design is presented. The generator show good performance at nominal load as well as for overloads. The first experimental results are published in this paper, mainly as a verification of the numerical code. Most work in this paper was carried out by the author.

Published online in 2006 and currently in press for *International Journal of Energy Research*.

Paper III: Verification of Cyclic Boundary Condition and 2D Field Model for Synchronous PM Linear Generator

Experimental results, from the prototype generator, is compared with results given by the numerical tool. The experimental results verify to a large

extent the numerical simulations. The first evidence of the the influence of the longitudinal ends where discovered during the work with this paper, which later on led to development of the analytical theory presented in paper V. The simulations and magnetic induction measurements are carried out by the author. The nominal speed voltages measurements where conducted by M. Stålberg.

Submitted September 2006 to *IEEE Transaction on Magnetics*.

Paper IV: First experimental results from sea trials of a novel wave energy system

The first results from the offshore trials are presented here. A study of the absorption factor, where data from 2.5 months is utilized, is presented. This paper is a team work of several authors. The extensive data treatment incorporated in the absorption study and most of the writing is carried out by R. Waters. The position and speed algorithm is constructed by the author.

Submitted September 2006 to *Applied Physics Letter*.

Paper V: Analytic model of flux distribution in linear PM synchronous machines including longitudinal end effects

This is a more theoretical paper, which investigates a phenomena discovered during the experiments on the prototype generator. The phenomena is a distortion in the magnetic flux distribution, caused by the longitudinal ends of the linear generator. An analytical model that describes the phenomena is developed and verified against FE-simulations. Hopefully, this paper could be the first in a series of papers, which explores the longitudinal end effects. Most work in this paper was carried out by the author.

Accepted 2006 to *IEEE Transaction on Magnetics*.

Paper VI: Electromagnetic forces in the air gap of a permanent magnet linear generator at no load

Paper VI and VII treats different aspects of the air gap forces in the generator. The problem with high normal forces in the air gap became evident in the experimental work with the prototype. In this paper the unstable equilibrium of the actuator is investigated. The resulting normal forces on an actuator for different displacements were calculated by finite element method. This paper gave input for the construction of the offshore generator. The simulations are carried out by K. Nilsson and the analytical verification is done by the author.

Published February 2006 in *Journal of Applied Physics*.

Paper VII: Measuring air gap width of permanent magnet linear generators using search coil sensor

This paper presents the design and experimental testing of a search coil sensor, which can monitor the air gap width in the generator. The aim was to develop a sensor system that could be used in an offshore wave energy converter and provide information about the air gap width during operation. The paper is based on Master thesis work performed by R. Waters. The author was the supervisor for this master thesis and coauthor of the paper.

Accepted 2006 to *Journal of Applied Physics*

Paper VIII: An electrical approach to wave energy conversion

This is a more general paper, which gives a thorough description of the entire wave converter system. The benefit of using an electric approach is highlighted. The research work on the linear generator is summarized, from FE-modeling to the first prototype. The paper is a joint effort. The experimental results are based on work performed by the author.

Published July 2006 in *Renewable Energy*.

Paper IX: Simulated Response of a Linear Generator Wave Energy Converter

The dynamic behavior of the plant is investigated in this paper. A first order hydrodynamic model is used, where only the displaced volume of water is taken into account. Nevertheless, the basic dynamics of the plant predicted by the model, coincide well with the results from the offshore experiments. From this paper, it was learned how the power absorption of the plant can be tailored for a specific wave climate by varying spring constants and buoy height. Most work in this paper was carried out by the author.

Reviewed conference paper. Presented 2004 at the *4th ISOPE Conference* by the author.

Paper X: A direct drive wave energy converter - Simulations and experiments

This paper gives a review of the wave energy project. The hydrodynamic modeling of a point absorber, the grid connection, and the generator is treated in different sections. This paper is a joint effort. The generator section is written solely by the author.

Reviewed conference paper. Presented 2005 at *24rd International Conference on Offshore Mechanics and Arctic Engineering* by the author.

11. Svensk sammanfattning

Energibehovet i världen växer stadigt. Samtidigt har vi börjat inse faran med att släppa ut mer koldioxid i atmosfären och varningstecken pekar på att oljeproduktionen inte kommer att kunna matcha den ökande oljekonsumtionen. Behovet av att hitta nya energikällor, som inte baseras på fossila bränslen, är således mycket stort.

En hittills outnyttjad källa till energi finns i våra hav. Vågkraft är en förnyelsebar energikälla med flera intressanta egenskaper, såsom hög energidensitet och hög utnyttjandetid. Dessutom kan vågkraft utvinnas med mycket liten miljöpåverkan och liten visuell störning. Rätt utnyttjad kan vågkraft bidra med en betydande del till världens energiproduktion. Utvinning av vågkraft innebär också ett flertal utmaningar, där de enorma krafterna som utvecklas vid en storm är en av de mest påtagliga.

Ett flertal tekniska lösningar har prövats genom åren, men än så länge har inget koncept bevisat sin ekonomiska lönsamhet. Ett stort problem är hållbarheten. Många vågkraftverk klarar inte de stora påfrestningar en storm innebär. Ett annat problem är att många utvecklare enbart fokuserar på ett steg i omvandlingskedjan och inte på helheten, vilket resulterar i ett dåligt fungerande system totalt sett.

Vid Uppsala Universitet studeras en ny typ av vågkraftverk där generatorn är direkt kopplad till en boj som drivs av vågorna. Istället för att anpassa vågkraftverket efter en konventionell, roterande generator, anpassas här generatorn till vågornas rörelse. Generatorn rör sig därför linjärt med låg hastighet.

Denna avhandling beskriver utvecklingen av en linjärgenerator för användning i vågkraftverk. De elektromagnetiska egenskaperna hos generatorn har undersökts med ett databaserat simuleringsverktyg. Simuleringarna, som bygger på finitelementmodellering av de magnetiska fälten, ger en mycket noggrann bild av generatorns elektriska egenskaper.

Utifrån simuleringarna har en första prototypgenerator konstruerats och testats i labbmiljö. Ett flertal experiment har genomförts, bland annat för att verifiera resultaten från simuleringsverktyget.

Den 13:e mars 2006 installerades det första vågkraftverksaggregatet på botten utanför Lysekil. Aggregatet har en effekt på 10 kW och den producerade elektriciteten överförs till land via en sjökabel. Sedan installationen har en rad mätningar genomförts. Till exempel har vågkraftverkets energiabsorption studerats för olika dämpningar och ett optimal dämpintervall har identifierats.

Detta arbete är en del av ett större projekt där olika aspekter av vågkraftverket studeras. Slutmålet är att få ett fungerande system, som på ett ekonomiskt och miljömässigt sätt kan producera elektricitet till elnätet.

12. Acknowledgment

Det finns många människor jag skulle vilja tacka för en massa saker. Här tänker jag bara tacka för sådant som har direkt anknytning till min doktorering. Om ni inte hittar er själva i listan, misströsta inte! Det betyder antagligen bara att ni till största del tillhör mitt privatliv och slipper mitt professionella liv.

Mats, min handledare, tack för detta äventyr. Tack för din uppmuntran och för att du får mig att lyfta blicken och se de verkliga problemen. Tack för ständigt pågående diskussioner och ditt plötsliga intresse för kommatering!

Karin N, ständiga rumskamrat och diskussionspartner. Tack för allt, men det är inte över än. Framför allt tack för din ovärderliga insats helgen innan tryckning!

Elisabeth, min första biträdande handledare. Jag lärde mig mycket av dig. Tack för din entusiasm och hjälp med de första artiklarna. När blir nästa slattrunda?

Urban, du fick delvis ta över jobbet som biträdande handledare. Tack för kloka råd i svåra frågor. Tack för hjälp med artiklar och med avhandlingen!

Rafael, lärjunge, sedermera sidekick. Nu får man stå bredvid och se dig glänsa... Tack för trevligt samarbete och hjälp med avhandlingen!

Karin T, tack för latex.com, läsning och annan problemlösning under skrivandet av avhandling. Dessutom, tack för en trevlig konferensresa!

Magnus, Micke, Richard och Hans, tack för samarbeten och tack för hjälp med genomläsning och diskussioner kring min avhandling!

Lysekilsgänget, tack för trevliga kvällar i friggebodar, på hamburgerhak och i whiskeysalonger, med stora drömmar om den perfekta generatorn!

Nelson, you always cheer me up and make me believe that I'm a good scientist. Thank you for the help with the thesis!

Arne och Karl-Erik, tack för allt ni har lärt mig om generatorer och simuleringar!

Ulf, Gunnel och Thomas, tack för hjälp med vardagliga bestyr som borttappade filer, krångliga gängor och besvärliga reseräkningar!

Alla på avdelningen, tack för den här tiden och för all hjälp jag har fått i stora och små frågor!

Erik, tack för den noggranna genomläsningen av introduktionen!

Bengt och Björn, tack för hjälp med referenser och annat för avhandlingen!

Britta och Torbjörn, tack för goda råd från er erfarna doktorer!

Min familj, tack för allt intresse, all uppmuntran och alla goda råd. Tack för all kärlek. Nu är jag snart i Mora!

Karin, tack för allt! Tack för muffins, tack för promenader, tack för diskussioner och genomläsning! Klokast och allra närmast är du!

Bibliography

[1] B. Söderbergh, F. Robelius, and K. Aleklett. A crash programme scenario for the canadian oil sands industry. *Energy Policy*, in press, 2006.

[2] R.L. Hirsch, R. Bezdek, and R. Wendling. Peaking of world oil production: Impacts, mitigation and risk management. *Energy Bulletin*, March 2005.

[3] P. O'Dell. *Why carbon fuels will dominate the 21st century's global energy economy*. Number ISBN: 0 906522 22 6. 2004.

[4] M. E. Mann, R. S. Bradley, and M. K. Hughes. Global-scale temperature patterns and climate forcing over the past six centuries. *Nature*, 392:779–787, 1998.

[5] A. Anders Moberg, D.M. Sonechkin, K. Holmgren, N.M. Datsenko, and W. Karlen. Highly variable northern hemisphere temperatures reconstructed from low- and high-resolution proxy data. *Nature*, 433:613–617, 2005.

[6] International Energy Agency. Share of total primary energy supply in 2003. Technical report, 2003.

[7] Energy Information Administration. Country analysis briefs, Chile. Technical report, 2005.

[8] International Energy Agency. *Natural Gas Market Review 2006 – Towards a Global Gas Market*. Number ISBN: 92-64-10984-6. 2006.

[9] H. Bernhoff, E. Sjöstedt, and M. Leijon. Wave energy resources in sheltered sea areas: A case study of the baltic sea. *Renewable Energy*, 31(13):2164–2170, 2006.

[10] U. Henfridsson, V. Neimane, K. Strand, R. Kapper, H. Bernhoff, O. Danielsson, M. Leijon, J. Sundberg, K. Thorburn, E. Ericsson, and K. Bergman. Wave energy potential in the baltic sea and the danish part of the north sea, with reflections on the skagerrak. *Submitted to Renewable Energy*, 2006.

[11] J. Falnes and K. Budal. Wave power conversion by point absorbers. *Norwegian Maritime Research*, 6(4):2–11, 1987.

[12] S. Salter. Power conversion systems for ducks. In *International conference on future energy concepts*, volume 171, page 100–108, 1979.

[13] A. Clément, P. McCullen, A. Falcaõ, A. Fiorentino, F. Gardner, K. Hammarlund, G. Lemonis, T. Lewis, K. Nielsen, S. Petroncini, M.T. Pontes, P. Schild, B.O. Sjöström, H.C. Sørensen, and T. Thorpe. Wave energy in europe: current status and perspectives. *Renewable and Sustainable Energy Reviews*, 6(5):405–431, 2002.

[14] M.C. Carcas. The opd pelamis wec: Current status and onward programme (2002). *International Journal of Ambient Energy*, 24(1):21–28, 2003.

[15] WEC. Renewable energy resources: Opportunities and constraints 1990-2020. Technical report, World Energy Council, 1993.

[16] M. Leijon, H. Bernhoff, M. Berg, and O. Agren. Economical considerations of renewable electric energy production — especially development of wave energy. *ERenewable Energy*, 28(8):1201–1209, 2003.

[17] Roger Bedard. Final summary report, project definition study, offshore wave power feasibility demonstration project. Technical Report E2I EPRI Global WP 009 – US Rev 1, 2005.

[18] M. Boukinda, V. Quiniou-Ramus, F. Schoefs, M. Birades, A. Lahaille, and R. Garetta. Marine growth colonisation process and profile in guinea gulf: From inspection data to load computing. In *24rd International Conference on Offshore Mechanics and Arctic Engineering, Jun 12-17 2005*, Proceedings of OMAE, Halkidiki, Greece, 2005.

[19] VICTOR L NEUENSCHWANDER. Wave activated generator. *US Patent*, (540602), 1985-09-03 1985.

[20] D. Ross. *Power from the Waves*. Oxford University Press, 1995.

[21] M.A. Mueller. Electrical generators for direct drive wave energy converters. *IEE Proceedings: Generation, Transmission and Distribution*, 149(4):446–456, 2002.

[22] H. Polinder, M.E.C. Damen, and F. Gardner. Linear pm generator system for wave energy conversion in the aws. *Energy Conversion, IEEE Transactions on*, 19(3):583–589, 2004.

[23] M. Leijon, H. Bernhoff, O. Agren, J. Isberg, J. Sundberg, M. Berg, K.E. Karlsson, and A. Wolfbrandt. Multiphysics simulation of wave energy to electric energy conversion by permanent magnet linear generator. *Energy Conversion, IEEE Transactions on*, 20(1):219–224, 2005.

[24] J. Falnes. Principles for capture of energy from ocean waves. phase control and optimum oscillation. Technical report, Institutt for fysikk, NTNU, 1995.

[25] Karin Thorburn, Hans Bernhoff, and Mats Leijon. Wave energy transmission system concepts for linear generator arrays. *Ocean Engineering*, 31(11-12):1339–1349.

[26] Mikael Eriksson. *Electromechanical Dynamics of a Direct Drive Wave Energy Converter*. Number UURIE 296-04L. 2004.

[27] Mikael Eriksson, Hans Bernhoff, Karin Thorburn, and Mats Leijon. Dynamics of a linear generator for wave energy conversion. In *23rd International Conference on Offshore Mechanics and Arctic Engineering, Jun 20-25 2004*, volume 3 of *Proceedings of the International Conference on Offshore Mechanics and Arctic Engineering - OMAE*, pages 545–549, Vancouver, BC, Canada, 2004. American Society of Mechanical Engineers, New York, NY 10016-5990, United States.

[28] M. Eriksson, J. Isberg, and M. Leijon. Hydrodynamic modelling of a direct drive wave energy converter. *International Journal of Engineering Science*, 43(17-18):1377–1387, 2005.

[29] Karin Thorburn. *Electric Energy Conversion Systems: Wave Energy and Hydropower*. Number ISBN 91-554-6617-6 in Comprehensive Summaries of Uppsala Dissertations from the Faculty of Science and Technology 202. 2006.

[30] Karin Thorburn. *Modelling new generators for wave energy conversion and hydropower upgrading*. Number UURIE 297-04L. 2004.

[31] R.L. Stoll. *The analysis of eddy currents*. Number ISBN 0 19 859311 2 in Monographs in Electrical and Electronic Engineering. Clarendon Press, Oxford, 19 edition, 1974.

[32] G. Bertotti. General properties of power losses in soft ferromagnetic materials. *Magnetics, IEEE Transactions on*, 24(1):621–630, 1988.

[33] K. Hameyer and R. Belmans. *Electrical machines and devices*. Advances in electrical and electronic engineering. WIT Press, 1999.

[34] O. Craiu, N. Dan, and E.A. Badea. Numerical analysis of permanent magnet dc motor performances. *Magnetics, IEEE Transactions on*, 31(6):3500–3502, 1995.

[35] A.B.J. Reece and T.W. Preston. *Finite Element Methods in Electrical Power Engineering*. Number 13 in Monographs in Electrical and Electronic Engineering. Oxford University Press, 2000.

[36] I.A. Tsukerman, A. Konrad, G. Meunier, and J.C. Sabonnadiere. Coupled field-circuit problems: Trends and accomplishments. In *Electromagnetic Field Computation, 1992. Digest of the Fifth Biennial IEEE Conference on*, 1992.

[37] E. Vassent, G. Meunier, A. Foggia, and J.C. Sabonnadiere. Simulation of induction machine operation using a step-by-step finite-element method. *Journal of Applied Physics Thirty-Fourth Annual Conference on Magnetism and Magnetic Materials, 28 Nov.-1 Dec. 1989*, 67(9, pt.2B):5809–11, 1990.

[38] R. Gupta, T. Yoshino, and Y. Saito. Finite element solution of permanent magnetic field. *Magnetics, IEEE Transactions on*, 26(2):383–386, 1990.

[39] Chunting Mi, G.R. Slemon, and R. Bonert. Minimization of iron losses of permanent magnet synchronous machines. In *Electrical Machines and Systems, 2001. ICEMS 2001. Proceedings of the Fifth International Conference on*, volume 2, pages 818–823 vol.2, 2001.

[40] I. Boldea and S.A. Nasar. Linear electric actuators and generators. *Energy Conversion, IEEE Transactions on*, 14(3):712–717, 1999.

[41] G. W. McLean. Review of recent progress in linear motors. In *Electric Power Applications, IEE Proceedings B*, volume 135, pages 380–416, 1988.

[42] SMHI. In situ measurements of significant wave height and zero down crossing period at Ölands södra grund (n:56°07´ e:16°68´). Technical report, Swedish Meterological and Hydrological Institute.

[43] H. Polinder, B.C. Mecrow, A.G. Jack, P.G. Dickinson, and M.A. Mueller. Conventional and tfpm linear generators for direct-drive wave energy conversion. *Energy Conversion, IEEE Transactions on*, 20(2):260–267, 2005.

[44] N.J. Baker. *Linear generators for direct drive marine renewable energy converters*. School of Engineering, University of Durham, 2003.

[45] H. Weh, H. Hoffmann, and J. Landrath. New permanent magnet excited synchronous machine with high efficiency at low speeds. In *International Conference on Electrical Machines*, pages 35–40, 1988.

[46] M.R. Harris, G.H. Pajooman, and S.M. Abu Sharkh. Comparison of alternative topologies for vrpm (transverse-flux) electrical machines. In *Proceedings of the 1997 IEE Colloquium on New Topologies for Permanent Magnet Machines, Jun 18 1997*, IEE Colloquium (Digest), pages 2–1, London, UK, 1996. IEE, Stevenage, Engl.

[47] M.R. Harris, G.H. Pajooman, and S.M. Abu Sharkh. The problem of power factor in vrpm (transverse-flux) machines. In *Electrical Machines and Drives, 1997 Eighth International Conference on (Conf. Publ. No. 444)*, pages 386–390, 1997.

[48] Z. Chen, E. Spooner, W.T. Norris, and A.C. Williamson. Capacitor-assisted excitation of permanent-magnet generators. *Electric Power Applications, IEE Proceedings-*, 145(6):497–508, 1998.

[49] N.J. Baker and M.A. Mueller. Permanent magnet air-cored tubular linear generator for marine energy converters,. In *IEE Power Electronics and Electrical Machines & Drives Conference*, Edinburgh, 2004.

[50] I. A. Ivanova, O. Ågren, H. Bernhoff, and Leijon M. Simulation of cogging in a 100kw permanent magnet octagonal linear generator for ocean wave conversion. In *Int. Symp. on underwater technology, Taipei, Taiwan*, 2004.

[51] O. Danielsson, K. Thorburn, M. Eriksson, and M. Leijon. Permanent magnet fixation concepts for linear generator. In *Fifth European Wave Energy Conference*, Cork, Ireland, 2003.

[52] L.H. De Medeiros, G. Reyne, and G. Meunier. Comparison of global force calculations on permanent magnets. *Magnetics, IEEE Transactions on*, 36(5):1215–18, 1998.

[53] M. Stålberg, R. Waters, M. Eriksson, O. Danielsson, K Thorburn, H. Bernhoff, and M. Leijon. Full-scale testing of pm linear generator for point absorber wec. In *6th EWTEC conference in Glasgow*, 2005.

[54] J. Sundberg and O. Langhamer. Environmental questions related to point-absorbing linear wave-generators: Impact, effects and fouling. In *6th EWTEC conference in Glasgow*, 2005.

[55] Stefan Gustafsson. Measuring of waves at islandsberg and literature survey of wave measurement technology. Technical Report UPTE F04048, Division for electricity and Lightning Research, Uppsala University, 2004.

[56] M. Eriksson, J. Isberg, and M. Leijon. Hydrodynamic modelling of a direct drive wave energy converter. *International Journal of Engineering Science*, 43:1377–1387, 2005.

[57] Zesheng Deng, I. Boldea, and S. Nasar. Fields in permanent magnet linear synchronous machines. *Magnetics, IEEE Transactions on*, 22(2):107–112, 1986.

[58] Jiabin Wang, D. Howe, and G.W. Jewell. Fringing in tubular permanent-magnet machines: Part i. magnetic field distribution, flux linkage, and thrust force. *Magnetics, IEEE Transactions on*, 39(6):3507–3516, 2003.

[59] I. Boldea and S.A. Nasar. *Linear electric actuators and generators*. Cambridge University Press, 1997.

[60] D. Deas, P. Kuo-Peng, N. Sadowski, A.M. Oliveira, J.L. Roel, and J.P.A. Bastos. 2-d fem modeling of the tubular linear induction motor taking into account the movement. *Magnetics, IEEE Transactions on*, 38(2):1165–1168, 2002.

[61] Henk Polinder, Johannes G. Slootweg, Martin J. Hoeijmakers, and John C. Compter. Modeling of a linear pm machine including magnetic saturation and

end effects: Maximum force-to-current ratio. *IEEE Transactions on Industry Applications*, 39(6):1681–1688, 2003.

[62] J. Faiz and H. Jagari. Accurate modeling of single-sided linear induction motor considers end effect and equivalent thickness. *Magnetics, IEEE Transactions on*, 36(5):3785–3790, 2000. 0018-9464.

[63] K. Adamiak, K. Ananthasivam, G.E. Dawson, A.R. Eastham, and J.F. Gieras. The causes and consequences of phase unbalance in single-sided linear induction motors. *Magnetics, IEEE Transactions on*, 24(6):3223–3233, 1988.

[64] J. F. Eastham, M. J. Balchin, and P. C. Coles. Full-scale testing of a high speed linear synchronous motor and calculation of end-effects. *Magnetics, IEEE Transactions on*, 24(6):2892–2894, 1988. 0018-9464.

[65] Jung Sang-Yong, Jung Hyun-Kyo, Chun Jang-Sung, Kim Do-Hyun, and Hwang Ji-Hyun. Dynamic characteristics of partially excited permanent magnet linear synchronous motor considering end-effect. pages 508–515, 2001.

[66] M. Platen and G. Henneberger. Examination of leakage and end effects in a linear synchronous motor for vertical transportation by means of finite element computation. *Magnetics, IEEE Transactions on*, 37(5):3640–3643, 2001.

Acta Universitatis Upsaliensis

Digital Comprehensive Summaries of Uppsala Dissertations from the Faculty of Science and Technology 232

Editor: The Dean of the Faculty of Science and Technology

A doctoral dissertation from the Faculty of Science and Technology, Uppsala University, is usually a summary of a number of papers. A few copies of the complete dissertation are kept at major Swedish research libraries, while the summary alone is distributed internationally through the series Digital Comprehensive Summaries of Uppsala Dissertations from the Faculty of Science and Technology. (Prior to January, 2005, the series was published under the title "Comprehensive Summaries of Uppsala Dissertations from the Faculty of Science and Technology".)

Distribution: publications.uu.se
urn:nbn:se:uu:diva-7194

ACTA
UNIVERSITATIS
UPSALIENSIS
UPPSALA
2006